On structure and primordial origin of black holes

Michael Zantedeschi

München 2022

On structure and primordial origin of black holes

Michael Zantedeschi

Dissertation
der Fakultät für Physik
der Ludwig-Maximilians-Universität
München

vorgelegt von
Michael Zantedeschi
aus Verona, Italy

München, den 09.06.2022

Erstgutachter: Prof. Gia Dvali
Zweitgutachter: Prof. Goran Senjanović
Tag der mündlichen Prüfung: 22.07.2022

Contents

List of Figures

Zusammenfassung

Das Verständnis der mikroskopischen Struktur Schwarzer Löcher bleibt eine der wichtigsten Aufgaben der theoretischen Physik. Besonders wertvoll ist es, wenn diese Struktur in Form von transparenten physikalischen Phänomenen mit beobachtbaren Konsequenzen formuliert werden kann. In der vorliegenden Dissertation diskutiere ich eine solche Idee. Konkret argumentiere ich für das Vorhandensein einer Wirbelsubstruktur in Schwarzen Löchern. Dies wird durch zwei verschiedene Paradigmen gestützt, die sich mit den Quanteneigenschaften von Schwarzen Löchern befassen. Das erste besteht aus einer Korrespondenz zwischen Schwarzen Löchern und generischen Objekten mit maximaler Entropie, die mit der Unitarität vereinbar sind, den so genannten Saturonen. In dieser Arbeit wird eine spezifische Realisierung des letzteren explizit ausgearbeitet. Bemerkenswerterweise ergeben sich aus der einfachen Anforderung der Unitaritätssättigung mehrere Eigenschaften, die denen von Schwarzen Löchern in einem einfachen Nicht-Gravitationsmodell entsprechen. Insbesondere wird eine Korrespondenz zwischen solchen Saturonen mit Wirbelstärke und nahezu extrem rotierenden schwarzen Löchern deutlich. Das zweite ist das so genannte N-Portrait, bei dem Schwarze Löcher als Kondensate von marginal begrenzten Gravitonen verstanden werden. Sowohl aus der ersten als auch aus der zweiten Sichtweise heraus liegt die Vermutung nahe, dass die Wirbelstärke eine notwendige Eigenschaft stark rotierender Schwarzer Löcher ist. Einerseits kann dies tiefgreifende astrophysikalische Konsequenzen haben, andererseits kann es aus der Perspektive vieler Körper von Interesse sein. Ersteres ist relevant für die starken Jets, die in aktiven galaktischen Kernen wie M87 beobachtet werden. Diese Emissionen können im Gegensatz zum Standardbild ohne eine kohärent magnetisierte Scheibe erklärt werden, was ein klares Indiz für das Szenario darstellt. Dieses Ergebnis ist generell für supermassereiche Schwarze Löcher in den galaktischen Zentren von Bedeutung, da diese aufgrund ihrer Spätzeitdynamik ein hohes Maß an Rotation aufweisen dürften und dies auch beobachtet wurde.

Der zweite Teil dieser Arbeit konzentriert sich auf leichtere Schwarze Löcher mit subsolarer Masse. Diese Objekte können nicht durch die Standard-Sterndynamik gebildet werden und würden, falls sie entdeckt werden, eine andere Erklärung für ihren Ursprung erfordern: Sie könnten zum Beispiel primordial sein. In diesem Fall sind diese Objekte phänomenologisch motivierte Kandidaten für dunkle Materie. Allerdings besteht derzeit kein Konsens über ihren Entstehungsmechanismus. Der Rest dieser Dissertation widmet sich daher der Vorstellung eines dieser Mechanismen sowie der daraus resultierenden Konsequenzen. In diesem Szenario bilden sich Schwarze Löcher durch den Einschluss von

Quarks, die im frühen Universum entstanden sind. Der Mechanismus erfordert nur eine minimale Hypothese, um sowohl in "unserem" QCD-Sektor als auch in einem dunklen Sektor zu funktionieren, wobei mehrere Probleme vermieden werden, die in den Standardentstehungsszenarien, die auf dem Kollaps inflationärer Überdichten basieren. Eine der Besonderheiten liegt in der natürlichen Produktion von hochgradig drehenden Schwarzen Löchern bei der Entstehung - relevant im Hinblick auf die zuvor diskutierte Wirbelunterstruktur. Eine weitere Eigenschaft ist die spezifische Gravitationswellen-Energiedichte, die durch die kollabierenden Dynamik erzeugt wird, die nahezu frequenzunabhängig ist. Das resultierende Spektrum kann möglicherweise den stochastischen gravitativen Hintergrund erklären der mit Pulsar-Timing-Arrays beobachtet wird, erklären und wird in naher Zukunft von anderen Beobachtungsmissionen untersucht werden die bei höheren Frequenzen arbeiten.

Motiviert durch die phänomenologische Relevanz wird eine numerische Studie der kollabierenden Dynamik von zwei eingeschlossenen Monopolen durchgeführt. Es wird erwartet, dass dies die Hauptmerkmale des zuvor erwähnten Quark-Kollapses erfasst. Ein Quark/Anti-Quark-Paar, das durch einen Gluon-String verbunden ist, ähnelt einem Monopol/Anti-Monopol-Paar, das durch ein magnetisches Flussrohr verbunden ist. Seit langem stellt sich die Frage, wie viel das letztere System über das erstere aussagen kann. Während diese Analyse die bereits bestehenden Studien über die Dynamik von eingeschlossenen Monopolen im punktförmigen Limit erweitert, liefert sie neue Erkenntnisse über die Korrespondenz mit der QCD-Physik. Interessanterweise spielt die Sättigung der Unitarität eine Schlüsselrolle, wenn es darum geht, Licht in diese Korrespondenz zu bringen.

Abstract

Understanding the microscopic structure of black holes remains one of the most important tasks of theoretical physics. It is especially valuable when this structure can be formulated in terms of transparent physical phenomena with observational consequences. In the first part of this dissertation, I discuss such an idea. Concretely, I argue for the presence of vortex sub-structure within black holes. This is supported by two different paradigms addressing the quantum properties of black holes. The first one consists of a correspondence between black holes and generic objects of maximal entropy compatible with unitarity, so-called saturons. In this work, a specific realization of the latter is worked out explicitly. Remarkably, from the simple requirement of unitarity saturation, several properties analogous to the ones of black holes emerge in a simple non-gravitational model. In particular, a correspondence between such saturons with vorticity and close-to-extremal rotating black holes is made apparent. The second one is the so-called N-portrait, where black holes are understood as condensates of marginally bounded gravitons. Motivated by both the former and the latter, it is natural to conjecture that vorticity is a necessary property of highly-spinning black holes. One one hand, this can have profound astrophysical consequences, and, on the other, it can be of interest from a many-body perspective. The former is relevant for powerful jets observed in active galactic nuclei such as M87. These emissions can be explained without the need of a coherently magnetized disk, contrary to the standard picture, providing a clear smoking gun for the scenario. This result is generally relevant for supermassive black holes in the galactic centres, since these are expected, and observed, to be highly spinning due to their late-time dynamics.

The second part of this thesis focuses on lighter, sub-solar mass black holes. Standard stellar dynamics cannot account for them and, if detected, an explanation for their origin would be required: for example, they could be primordial. These objects are phenomenologically motivated dark matter candidates. However, there is currently no consensus on their formation mechanism. The rest of this dissertation is therefore dedicated to presenting one of those mechanisms, as well as its consequences. In this scenario black holes are formed due to confinement of quarks produced in the Early Universe. The mechanism requires minimal hypothesis to work both within "our" QCD sector or in a dark sector, while avoiding several issues encountered in the standard formation scenarios based on the collapse of inflationary overdensities. One of its peculiar features lies in the natural production of highly spinning black holes at formation – relevant in view of the previously discussed vortex sub-structure. Yet another property is the specific gravitational-wave energy density produced by the collapsing dynamics, which is almost frequency-independent. The resulting spectrum can potentially explain the stochastic gravitational background observed via pulsar timing arrays and will be probed in the near future by other observational missions operating at higher frequencies.

Motivated by the phenomenological relevance, a numerical study of the collapsing dynamics of two confined monopoles is performed. This is expected to capture the main features of the previously mentioned quark collapse. In fact, a quark/anti-quark pair connected by a gluon string is similar to a monopole/anti-monopole pair connected by a magnetic flux tube. A long-standing question is how much the latter system can inform us about the former. Therefore, while this analysis extends previous studies on the dynamics of confined monopoles performed in the point-like limit, it provides new insights on its correspondence with QCD physics. Intriguingly, unitarity saturation plays a key-role in shedding light on such correspondence.

List of Publications and preprints

This thesis is based on a series of ongoing projects, of which some results have already been published:

1. Dvali Gia, Florian Kühnel, and Michael Zantedeschi. "Vortexes in Black Holes." arXiv:2112.08354 (2021).
2. Dvali Gia, Florian Kühnel, and Michael Zantedeschi. "Primordial black holes from confinement." Physical Review D 104, no. 12 (2021): 123507.
3. Dvali Gia, Juan Valbuena Bermudez, and Michael Zantedeschi. "Dynamics of confined monopoles." To appear.

A substantial part of this manuscript, therefore follows from collaborations with Gia Dvali, Florian Kühnel and Juan Valbuena Bermudez and is, to a large extent, an ad verbatim reproduction of the text, figures and equations of those articles. What this work tries to achieve is to put those results in a wider context, while providing, at the same time, the necessary background within a unifying picture.

Other articles published or posted during the doctoral period, not discussed here, are

- Kovtun Andrei, and Michael Zantedeschi. "Breaking BEC." Journal of High Energy Physics 2020, no. 7 (2020): 1-24.
- Kovtun Andrei, and Michael Zantedeschi. "Breaking BEC: Quantum evolution of unstable condensates." Physical Review D 105, no. 8 (2022): 085019.
- Berezhiani Lasha, Giordano Cintia, and Michael Zantedeschi. "Background-field method and initial-time singularity for coherent states." Physical Review D 105, no. 4 (2022): 045003.
- Berezhiani Lasha, and Michael Zantedeschi. "Evolution of coherent states as quantum counterpart of classical dynamics." Physical Review D 104, no. 8 (2021): 085007.
- Preda Anca, Goran Senjanović, and Michael Zantedeschi. "SO (10): a Case for Hadron Colliders." arXiv:2201.02785 (2022).

- Senjanović Goran, and Michael Zantedeschi. "$SU(5)$ grand unification and W-boson mass." arXiv:2205.05022 (2022).

Chapter 1

Invitation

1.1 Black Holes

Black holes (BHs) are the main focus of this work. Therefore, before proceeding, we shall review some of their properties. A Schwarzschild BH is a solution of Einstein's General Relativity with metric

$$ds^2 = -\left(1 - \frac{r_g}{r}\right) dt^2 + \left(1 - \frac{r_g}{r}\right)^{-1} dr^2 + r^2 d\Omega^2, \tag{1.1}$$

where $r_g = 2G_N M$ is the Schwazschild radius, M the BH mass and $d\Omega^2$ is the two-sphere distance. The Schwarzschild radius determines the event horizon. This is the sphere from which no light-like worldline can escape from.

BHs are considered exceptional objects due to their mysterious properties such as their area-law entropy [1], the presence of an information horizon, a thermal spectrum – known as Hawking radiation [2]–, an information time retrieval i.e. a timescale after which the information stored by the BH becomes available to an asymptotic observer known as Page's time [3], a maximal bound on their spin, etc.

However, it was recently proposed that these properties are not unique to gravity, and to BHs [4]. This is due to the fact that unitarity imposes a universal bound on entropy [5]. This crucial observation followed from earlier works [6, 7] where configurations with high micro-state degeneracy were built while keeping unitarity under control.

The maximal entropy of a self-sustained localized configuration, gravitational or not, compatible with unitarity corresponds to [4]

$$S \leq \frac{Area}{G_{\text{Gold}}} = f^2 Area, \tag{1.2}$$

where $Area \sim R^{d-2}$, d being the spacetime dimensionality, corresponds to the area of the objects (from now on $d = 4$), and $G_{\text{Gold}} \sim f^{-2}$ is the Goldstone coupling associated to the symmetry broken by the object itself. Configurations saturating bound (1.2) are called saturons [4]. In particular, BHs are gravitational saturons spontaneously breaking Poincaré symmetry, whose Goldstone coupling is given by $G_{\rm N}$. Under the replacement

$$G_{\rm Gold} \to G_{\rm N}, \quad \text{equivalently} \quad f \to M_{\rm Pl}, \tag{1.3}$$

(1.2) reduces to the known Bekenstein entropy relation [1]

$$S_{\rm BH} \sim \frac{Area}{G_{\rm N}} \sim M_{\rm Pl}^2 Area. \tag{1.4}$$

Simultaneously, for saturons the entropy is also equal to

$$S_{\max} \sim Area\, G_{\rm Gold} \sim \frac{1}{\alpha}, \tag{1.5}$$

α being the value of the microscopic coupling in the theory at lengths R. For a BH $\alpha = \alpha_{\rm gr} \sim (R_{\rm BH} M_{\rm Pl})^{-2}$, which when inserted in (1.5), correctly recovers (1.4) ($G_{\rm N} = M_{\rm Pl}^{-2}$).

In [4, 5] it was shown that saturons, from a single requirement of entropy saturation, manifest several BH properties

- Indeed an area-law entropy (1.2)
- They decay, at leading order in $1/S$ in a thermal way

$$T \sim 1/R \tag{1.6}$$

- Semi-classically they display an information horizon
- A bound from below on their information retrieval (analogous to Page's time)

$$t_{\min} \sim \frac{R}{\alpha} \sim S_{\max} R. \tag{1.7}$$

- A bound on their maximal spin [8]

$$J_{\max} \leq S_{\max}. \tag{1.8}$$

  This is analogous to the maximal rotation of a spinning BH. Such object can be described in terms of Kerr metric and is uniquely determined by its mass M and its angular momentum J. In Boyer-Lindquist coordinates its metric reads

$$\begin{aligned} ds^2 = -\left(1 - \frac{r_g r}{\Sigma}\right) dt^2 + \frac{\Sigma}{\Delta} dr^2 + \Sigma d\theta^2 + \left(r^2 + a^2 + \frac{r_g r a^2}{\Sigma}\sin^2\theta\right)\sin^2\theta\; d\phi^2 \\ - \frac{2 r_g r a \sin^2\theta}{\Sigma} dt\, d\phi \end{aligned} \tag{1.9}$$

where the coordinates r, θ, ϕ are determined by

$$\begin{aligned} x &= \sqrt{r^2+a^2}\sin\theta\cos\phi, \\ y &= \sqrt{r^2+a^2}\sin\theta\sin\phi, \\ z &= r\cos\theta, \end{aligned} \tag{1.10}$$

and the quantities

$$\begin{aligned} a &= \frac{J}{Mc}, \\ \Sigma &= r^2 + a^2\cos^2\theta, \\ \Delta &= r^2 - r_g r + a^2, \end{aligned} \tag{1.11}$$

were introduced for simplicity. The event horizon corresponds to the larger root of the condition $\Delta = 0$, for which the radial part of the metric becomes singular (analogously to the non-rotating case (1.1). Clearly, for $r_g < 2a$, or equivalently, $J > GM^2$, no real solution exist. Without an event horizon, the singularity of the BH becomes naked and this is not possible. It follows that, for a spinning BH

$$J_{BH} < GM^2 \simeq S_{BH}. \tag{1.12}$$

This is the gravitational version of (1.8). In the context of General Relativity, it emerges as a consequence of geometry. One of the main point of this work is that saturons outside of gravity obey the same bound. Its origin within these solution is clear and understood with standard field theoretical treatments as shown in [8].

The main message of Ref. [4] is that none of these properties are unique to BHs and to gravity. This connection has been shown for several models, such as instantons, solitons and other bound states [4, 6, 7, 5], eg., for $1+1$ dimensions [9] in the Goss-Neveu model [10]. Moreover, similar properties have been argued to emerge in QCD [11] in the so-called color-glass condensate [12].

As already mentioned, the case of spin for this class of objects has been firstly address in [8], which will be the main focus of this chapter. The main concept of vorticity was shown for a $SU(N)$ prototype model introduced in [4], and developed in [5] for the non-rotating case. These bound-states can be viewed as a special version of non-topological solitons, or Q-balls [13, 14]. An important new feature that makes them black-hole-like, is the maximal degeneracy of microstates which satisfies (1.2).

1.2 The role of saturation

Given the close relation between the entropy-area law and the saturation of unitarity, we recap here the main findings of Ref. [4], which will prove useful for later reference.

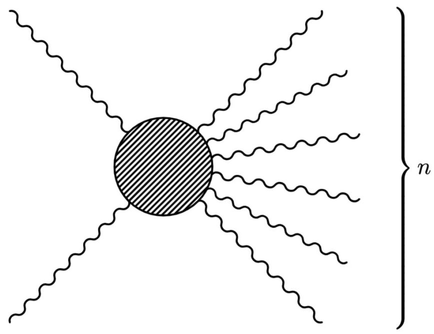

Figure 1.1: A $2 \to n$ process

It turns out [4] that unitarity of scattering amplitude puts a non-perturbative upper bound on the entropy of a system. The entropy bound attained by various field theoretical objects, was observed [6, 7] to be

$$S_{max} = MR = \frac{1}{\alpha} = Area\, f^2, \tag{1.13}$$

where $\mathcal{O}(1)$ factors have been dropped. We will explain how these equalities comes about below. The main message, is that the first two equality are deeply connected to scattering amplitudes. Namely, when the first two equality are satisfied by a field theoretical configuration, the system is in correspondence with the non-perturbative saturation of unitarity of a $2 \to n$ amplitude at momentum transfer $q = 1/R$ and $\alpha n = 1$. Moreover, in all practical explicit realizations where the first two equalities of (1.13) are satisfied, also the third condition applies. Namely, Bekenstein entropy follows from non-perturbative saturation of unitarity in $2 \to n$ scatterings.

This suggests the physical interpretation that at saturation, scattering of two highly energetic quanta can produce a classical object, namely a saturon via the process (see Fig. 1.1)

$$2 \to n = \textit{ saturon}. \tag{1.14}$$

This is somewhat counterintuitive, since the scattering of two highly-energetic quanta into a large number of soft-quanta is exponentially suppressed. The point is that a large number of final, physically equivalent microstate can make up for such suppression, providing a close-to-unity cross-section.

This is similar to what is expected for BHs. In fact, upon scattering of two arbitrarily highly energetic quanta (above M_p), a classical configuration, a BH satisfying relation (1.13), forms. Therefore a BH is an example of saturon in gravity. Notice that a BH forms regardless of the specific value of the scattering energy, as long as it is super-Planckian. The reason for this lies in the derivative-like nature of the gravitational coupling

$$\alpha_g(q) = \frac{q^2}{M_p^2}, \tag{1.15}$$

where q represents the typical momentum transfer of the $2 \to n = BH$ scattering at $q = 1/R$. When building saturons outside of gravity, e.g., in renormalizable theories, the microscopic coupling $\alpha(q)$ runs at most logarithmically. Therefore, it is not surprising that the saturation of unitarity, and therefore (1.13), is satisfied only at a specific center of mass energy. Namely, for a $2 \to n$ scattering, the typical momentum transfer depends on the microscopic coupling evaluated at that scale

$$q = \frac{1}{R} = f\sqrt{\alpha(1/R)}. \tag{1.16}$$

Correspondingly the center of mass energy is

$$E = qn = \frac{1}{R}n = f\sqrt{\alpha(1/R)}n. \tag{1.17}$$

The window of opportunity for this to happen has to be very narrow in the center of mass energy [4] $\Delta E/E \sim \alpha \ll 1$ [4]. From now on, the energy scale at which the coupling is evaluated is omitted.

1.2.1 Entropy relation to inverse coupling

To clarify the statements of the previous Section we believe instructive, and useful for later, to report here the example presented in [4].

Consider the following four-point bosonic interaction

$$\alpha(\phi_i\phi_i)(\phi_j\phi_j), \tag{1.18}$$

of a theory invariant under an internal symmetry acting on the index $i, j = 1, ..., N$. In the rest of the work we focus on the case of a weak microscopic coupling. Therefore, it is useful to define the following 't Hooft coupling [15]

$$\lambda_t = \alpha N, \tag{1.19}$$

and work in the double scaling limit

$$\alpha \to 0, \quad N \to \infty, \quad \lambda_t = finite. \tag{1.20}$$

We are interested into the scattering of two quanta into a highly occupied state of momentum $\vec{k}$ i.e.

$$|n\rangle = \prod_j \frac{\left(a_j^\dagger(\vec{k})\right)^{n_j}}{\sqrt{n_j!}}|0\rangle, \tag{1.21}$$

wherew a_j denotes the annihilation operator of the bosonic field in (1.18) and the total occupation number is

$$n = \sum_{j=1}^{N} n_j. \tag{1.22}$$

While the macrostate is fixed by n, its degeneracy can be large as it can be seen from its microstates realization (1.21). The reason for their indistinguishability is precisely due to the double-scaling limit (1.20).

Yet another coupling useful in this analysis, is the one due to the state (1.21), i.e. the collective coupling, describing the effective interaction between one quanta, and the background formed by the others

$$\lambda_c = \alpha n, \tag{1.23}$$

which is also taken in a double scaling limit

$$\alpha \to 0, \quad n \to \infty, \quad \lambda_c = finite. \tag{1.24}$$

In this limit, only leading order semiclassical corrections to the dynamics should be included [16, 17] and, however, they won't matter for the discussion [1].

For $n \gg 1$, the occupation number state (1.21) can be used to build explicitly the coherent state describing the energy lump. Notice that in this limit, the number eigenstate in (1.21), can be thought almost as a coherent state of n quanta, with energy per-constituent-quantum sharply peaked around $|\vec{k}| \sim 1/R \sim q$, q being the typical momentum transfer of the $2 \to n$ scattering amplitude. Therefore, this configuration is made of n constituent of energy $\sim q \sim 1/R$. Namely, the energy of the lump is

$$E \sim \frac{n}{R}. \tag{1.25}$$

For the system to be self-sustained, the kinetic energy of a single quantum should be balanced by the potential energy of the background i.e.,

$$E_{kin} \sim \frac{1}{R} \sim E_{pot} \sim \frac{\alpha n}{R}, \tag{1.26}$$

which holds true for

$$\lambda_c \sim 1. \tag{1.27}$$

Namely, a collective coupling of $\lambda_c \sim \mathcal{O}(1)$ is necessary. In this case the energy of the configuration is

$$E \sim \frac{n}{R} \sim \frac{1}{\alpha R}, \tag{1.28}$$

which is the usual relation between the size and the energy of a soliton.

Let us now turn to the entropy of the lump. In the limit $\alpha \to 0$ the microstates defining the macrostate (1.21) are classically indistinguishable. This is because in this limit, any process distinguishing the flavour (the j-index) of the particles is suppressed. This is the power of the large N limit.

[1] For example this effect should be accounted by a non-trivial transformation of the bosonic creation/annihilation operators via a Bogoliubov transformation.

In this limit the state in (1.21), under the constraint (1.22), has the following microstate degeneracy

$$n_{st} \simeq \binom{n+N}{N} = c_N \left(1+\frac{N}{n}\right)^n \left(1+\frac{n}{N}\right)^N , \tag{1.29}$$

where Stirling approximation was used for $n \gg 1$ and $N \gg 1$. Note that the prefactors c_N is a polynomial function of n, N and will not matter for the discussion. It can be set to one from here onwards.

The entropy of the configuration is given by ($\lambda_c = 1$)

$$S = \ln n_{st} \simeq \frac{1}{\alpha} \ln \left((1+\lambda_t) \left(1+\frac{1}{\lambda_t}\right)^{\lambda_t} \right) , \tag{1.30}$$

which reproduces the first two equalities of (1.13) for $\lambda_t \sim 1$. (c.f. (1.28)). Note that to obtain them, the theory required

$$\lambda_t \sim \lambda_c \sim 1. \tag{1.31}$$

The last equality in (1.13), is obtained by noticing that the lump breaks translation invariance, with associated Goldstone decay constant

$$f = \frac{1}{R\sqrt{\alpha}} = \frac{\sqrt{N}}{R}. \tag{1.32}$$

This shows that for unitary collective couplings (1.31), Bekenstein area-law (1.13) is recovered for this simple non-gravitational system.

1.2.2 The role of unitarity in scattering amplitudes

We are now ready to show the importance of saturation for the scattering amplitude of $2 \to n$ processes [4]. The relevant cross section is given by

$$\sigma = \sum_{microstates}^{n_{st}} \sigma_{2\to n}. \tag{1.33}$$

The last term corresponds to

$$\sigma_{2\to n} = c_n n! \alpha^n , \tag{1.34}$$

Similarly to before, the dimensionfull prefactor c_n is at most polynomial and not relevant for the discussion since here we are interested in the exponential behaviour of the cross-section.

Eq. (1.34) seems to grow unboundedly for large enough n. Such growth is not physical and is due to the asymptotic nature of the perturbative expansion in (1.34). Indeed, the point of optimal truncation is given by the n such that the succession in (1.34) stops decreasing and starts growing. This is given by

$$\lambda_c = \alpha n = 1, \tag{1.35}$$

for which, in the double-scaling limit (1.24)

$$\sigma_{2\to n} = e^{-n} = e^{-1/\alpha}, \tag{1.36}$$

as expected for the scattering amplitude associated to a $2 \to n$ process. It can be shown that (1.36) represents the maximal cross section also when non-perturbative effects are taken into account (i.e. for $n \gg \alpha^{-1}$) as shown by Ref. [4].

So far, the information about the microstates degeneracy has not been accounted. This appears in the form of summation of indistinguishable final states in (1.33). For $\lambda_c \sim \lambda_t \sim 1$, the resulting cross section becomes

$$\sigma \simeq e^{-\frac{1}{\alpha}+S}, \tag{1.37}$$

which is of order unity for $S = 1/\alpha$. This is precisely condition (1.13) obtained in the previous section. If the 't Hooft coupling $\lambda_t \gg 1$, the entropy would be bigger, but it would result in a violation of unitarity. This brings a clear message. Unitarity of $2 \to n$ scattering amplitudes puts an upper bound on the maximal entropy of a n-composite self-sustained configuration, which corresponds to (1.13).

1.3 The N-portrait

So far, a class of self-sustained configurations outside of gravity, sautrons, have been discussed. These objects saturate the unitarity bound of $2 \to n$ scattering amplitudes of 2 highly energetic quanta into n soft quanta due to the large microstate degeneracy of identical final states. It turns out that saturons, from this simple property, posses both an entropy-area law, as well as other several properties analogous to BH. The emergence of other properties other than Bekenstein area-law will be shown explicitly in the next chapter.

In this section we briefly summarize a a different approach which tries to resolve the inner substructure of BHs as a Bose-Einstein condensate of marginally bounded gravitons. This framework, proposed by Dvali and Gomez (see [18, 19, 20] for an incomplete list), is well-supported by the previously presented saturon picture. Historically, however, the latter came after the former.

A natural question is whether the microscopic substructure, which is better under-control, of non-gravitational saturon, could be extended to BHs. In fact saturons are localized classical self-sustained configurations composed of soft-quanta. In the case of a BH such soft quanta would be gravitons, and the system would be analogous to a Bose-Einstein condensate. The point is that, if this description holds true, then it bears corrections beyond the semi-classical treatment.

In this picture the number of constituents N is given by

$$N \simeq \frac{M^2}{M_p^2} \simeq \frac{R^2}{L_p^2}, \tag{1.38}$$

R being the BH Schwarzschild radius and M its mass. Each constituent has energy $q \sim 1/R$, therefore leading to the configuration mass

$$M = qN, \tag{1.39}$$

and the microscopic coupling is

$$\alpha_g = \frac{1}{M_p^2 R^2}. \tag{1.40}$$

Note the analogy between these equations and the one in the previous section. Hawking emission is understood in this picture as rescattering of constituent-quanta, composing the BH. To compute it, it is necessary to take into account the combinatorial factor, due to the presence of N-background gravitons. Moreover, the outgoing quanta have an energy given by the typical size of the localized object. This leads to

$$\Gamma \sim \alpha_g^2 \binom{N}{2} \frac{1}{R} \sim \frac{1}{R}, \tag{1.41}$$

where the binomial factor accounts for the above mentioned combinatorial factor ($N \gg 1$ was used), α_g is the coupling entering the Feynman diagram and R^{-1} is the typical energy.

The reason why this emission is thermal, i.e. $T \sim 1/R$, can be understood from the fact that for much more highly energetic quanta, $\delta N \gg 1$ condensate constituents takes part in the scattering. This process, is therefore exponentially suppressed as

$$e^{-\delta N} = e^{-\frac{\Delta E}{T}}, \tag{1.42}$$

where the typical energy of outgoing quanta is $\Delta E \sim \delta N/R$. Suppression (1.42) is precisely the Boltzmann factor expected for a thermal distribution.

In this construction, the classical BH is obtained in the limit of infinite constituents $N \to \infty$. It is clear that physical BHs have a finite N, and therefore $1/N$-corrections, not visible in semi-classical treatment, can be computed. These appear in the form of quantum hair, which becomes available to an asymptotic observer in a timescale

$$\Gamma^{-1} \sim \tau \sim \frac{R}{\alpha} \sim nR. \tag{1.43}$$

Two comments are in order: the above timescale corresponds to the celebrated Page time [3]. Classically it corresponds to the time after which the BH lost half of its mass due to the emission of Hawking quanta.

In the corpuscular picture it is the timescale after which the quantum backreaction is no longer negligible, as it becomes comparable to the mass of the BH itself. Therefore, it marks the timescale after which the semiclassical solution is no longer a reliable description of the BH. This is known as quantum breaking [20], and the timescale in (1.43) is the quantum break time (see Fig. 1.2 for a visual sketch of the phenomenon). Note that in the semi-classical limit, $n \to \infty$, τ also becomes infinite, exemplifying the quantum nature of the phenomenon[2].

[2] Restoring $\hbar$, $n \propto \hbar^{-1}$.

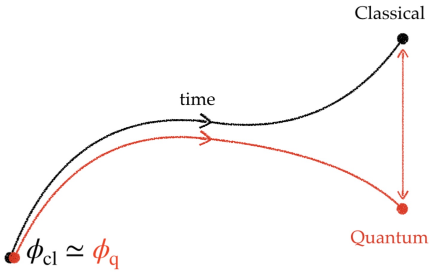

Figure 1.2: Dynamical trajectories of classical vs quantum one point function. At initial times the classical dynamics is a good approximation to the true quantum dynamics. At later time, the classical solution no longer provides a reliable description of the system.

This phenomenon was studied explicitly in several theories outside of gravity. For example, for the case of scalar field theories I worked out in depth the effect of quantum backreaction on coherent states – the quantum counterpart of classical configurations – both analytically [16, 17] and numerically [21, 22], within the framework of two-particle-irreducible effective actions. The main focus of these works were scalar homogeneous condensates.

Chapter 2

Vorticity in black holes

This chapter is based on my work with G. Dvali, F. Kühnel [8]. Therein we show that an analogous version of the extremality bound on the spin obeyed by a black hole is equally respected by a Q-ball type saturon within a renormalisable theory without gravity. This is achieved building an explicit stationary configuration with vorticity. Remarkably, the topological nature of the vortex winding, forbids the emission of soft quanta, therefore providing a microscopic understanding of the absence of Hawking-emission in extremal black hole. These features provide support for describing a black hole with maximal spin as a condensate of gravitons endowed with vorticity.

A generic consequence, is that in the presence of mobile charges, the global vortex traps the magnetic flux of the gauge fields, possibly providing macroscopically-observable consequences. This can explain, for example, the most powerful jests observed in active galactic nuclei, even without a specifically magnetized accretion disk surrounding the black hole. Such flux entrapment, can also serve as a probe to various hidden sectors, e.g., millicharged dark matter.

After introducing the subject, in this Chapter I will first recap on saturons and their physical relation to BHs, to later focus on the rotational case and the possible phenomenological consequences

2.1 Introduction

The microscopic structure of black holes remains to be understood. One of the main obstacles is the lack of experimental probes of black hole quantum properties. In this light, it is very important to identify and explore those microscopic theories that lead to macroscopically-observable phenomena. In this chapter I will describe one such phenomenon: vorticity [8]. Our proposal is based on two lines of thought.

On one hand, as discussed in the previous chapter, there are physical indications [19, 18] that at the quantum level a black hole of radius R represents a condensate of "soft" gravitons, i.e., gravitons of characteristic wavelength $\sim R$ and frequency

$$\omega \sim 1/R \,. \tag{2.1}$$

The defining property of a black hole is that the graviton condensate is at the critical point of saturation, also referred to as the point of "maximal packing". At this point, the occupation number of gravitons $N_{\rm gr}$, their quantum gravitational coupling (we shall work in $3+1$ dimensions),

$$\alpha_{\rm gr} \equiv 1/(RM_{\rm P})^2 \,, \quad M_{\rm P} \equiv \text{Planck mass} \,, \tag{2.2}$$

and entropy S, satisfy the relation

$$S = N_{\rm gr} = \frac{1}{\alpha_{\rm gr}} \,. \tag{2.3}$$

Taking into account Eq. (2.2), it is clear that this equation, reproduces the Bekenstein-Hawking entropy of a black hole.

On the other hand, it has been argued recently [4], and showed in the previous Chapter, that the expression (2.3) is not specific to black holes or gravity. Rather, it represents a particular manifestation of the following universal upper bound, imposed by unitarity, on the microstate entropy S of a generic self-sustained bound state of size R,

$$S = \frac{1}{\alpha} = R^2 f^2 \,, \tag{2.4}$$

where α is the running coupling of the theory evaluated at the scale R and f is the decay constant of Goldstone modes of symmetries spontaneously broken by the bound state. Furthermore, it was argued that there exists a large class of objects saturating this bound and that such objects, so-called saturons, exhibit close similarities with black holes. This proposal has been verified on multiple examples [6, 7, 4, 9, 5]. The correspondence between black holes and generic saturated systems opens up the possibility of using saturons in calculable theories as laboratories for understanding the well-established black hole properties and for predicting new ones.

The goal of the present chapter is to provide one more link in this correspondence. The main message is that black holes and other saturons naturally support a vortex structure. This imposes an upper bound on the saturon spin very similar to the extremality bound on a spinning black hole. This offers a microscopic explanation of black hole's maximal spin in terms of the vorticity of the graviton condensate.

The vortex structure, when interacting with a neutral plasma of particles charged under some gauge symmetry, such as electromagnetism, necessarily traps a magnetic flux in it. This trapping can have some macroscopically-observable consequences. It can also provide an observational window in various hidden sectors, such as millicharged dark matter.

We believe that, due to the universality of saturons, the vorticity property in black holes can be understood without entering into the technicalities of quantum gravitational computations. In short, at the level of our presentation, the vorticity in black holes represents a conjecture supported by the evidence gathered from calculable saturated systems.

We shall explain the main concepts on a prototype $SU(N)$ model [4] which has been shown by Ref. [5] to support the black-hole-like saturated bound-states. These bound-states can be viewed as a special version of non-topological solitons, or Q-balls [13, 23] (for some implications, see Refs. [14, 24]). An important new feature that makes them black-hole-like, is the maximal degeneracy of microstates which satisfies Eq. (2.3).

2.2 Prototype model

Consider a theory [4, 5] of a scalar field ϕ in the adjoint representation of global $SU(N)$ symmetry. The Lagrangian density in obvious matrix notations has the following form,

$$\mathcal{L} = \frac{1}{2}\mathrm{tr}(\partial_\mu\phi)(\partial^\mu\phi) - \frac{\alpha}{2}\mathrm{tr}\Big(f\phi - \phi^2 + \frac{I}{N}\mathrm{tr}\phi^2\Big)^2 . \tag{2.5}$$

Here, α is a dimensionless coupling and f is the scale. It is very important to keep in mind that α and N obey the unitarity constraint [4] described in the previous Chapter

$$\lambda_t = \alpha N \lesssim 1 . \tag{2.6}$$

The correspondence with a macroscopic black hole pushes one to consider the extremely large values of N (for instance, considering a solar-mass black hole leads to $N \sim 10^{77}$). This gives the benefit of using the power of $1/N$-expansion and we will work, from now on, to leading order in $1/N$.

The theory (2.5) has multiple degenerate vacua with different patterns of spontaneous symmetry breaking as seen from the minimization equation

$$f\phi_a^b - \Big(\phi^2\Big)_a^b + \frac{\delta_a^b}{N}\mathrm{tr}\phi^2 = 0 \tag{2.7}$$

These vacua corresponds to the breaking of $SU(N) \to SU(N-K)\times SU(K)\times U(1)$, for $N \geq K \geq 1$. The order parameters breaking to these vacua can be parametrized as

$$\langle\phi\rangle = \langle\varphi\rangle\frac{\sqrt{K}}{\sqrt{N(N-K)}}\mathrm{diag}\left(\frac{N-K}{K},...,\frac{N-K}{K},-1,...,1\right), \tag{2.8}$$

where the traceless diagonal vacuum matrix contain respectively K and $N-K$ identical elements, corresponding to $(N-K)/K$ and -1 above. The broken generators by this configuration correspond to the ones living in the off-diagonal block matrix. A simple counting gives $2(N-K)K$ broken generators, where $(N-K)K$ is the size of the mentioned off-diagonal block matrix, and the factor two is due to the presence of two generators for each entry (the analog of σ_1 and σ_2 Pauli matrices distributed in the block).

Inserting ansatz (2.8) in the vacuum condition (2.7), we obtain

$$\langle\varphi\rangle = f\frac{\sqrt{K(N-K)}}{N-2K}. \tag{2.9}$$

For the present discussion focus will be on the $SU(N)$-symmetric vacuum and the broken one $SU(N-1) \times U(1)$ i.e., $K = 1$. In the former vacuum, the theory exhibits a mass gap $m^2 = \alpha f^2$. In the latter, for $N \gg 1$, there exist $\simeq 2N$ species of massless Goldstone modes and $\langle\varphi\rangle \simeq f$. The two vacua are separated by a domain wall. A planar static wall has a tension (energy per unit length) equal $m^3/6\alpha$. The thickness of the wall is $\delta_{\mathrm{w}} = 1/m$.

Following Ref. [5], we shall be interested in the field configurations described by the ansatz

$$\phi = U^\dagger \Phi U \,, \tag{2.10}$$

where (for $N \gg 1$)

$$\Phi = \frac{\rho(x)}{N} \mathrm{diag}\Big[(N-1), -1, \dots, -1\Big] \,, \tag{2.11}$$

and

$$U = \exp\Big[i\,\chi^a(x) T^a\Big] \,. \tag{2.12}$$

Here T^a's are the generators broken by Eq. (2.11) and $\chi^a(x)$ are the corresponding Goldstone mode. This ansatz gives the effective Lagrangian ($1/N$ effects absorbed in rescalings)

$$\mathcal{L} = \frac{1}{2}\Big[\partial_\mu \rho \partial^\mu \rho + \rho^2 \partial_\mu \chi^a \partial^\mu \chi^a - \alpha \rho^2 (\rho - f)^2\Big]. \tag{2.13}$$

In this effective theory, we shall be interested in the state that represents a hybrid of the following two solutions.

The first solution [5], which serves as the basis for the black hole prototype, is a stationary spherical bubble of $SU(N-1) \times U(1)$ vacuum embedded in $SU(N)$-invariant asymptotic space. This solution is described by the ansatz,

$$\rho = \rho(r) \,, \;\; \chi^a = \delta^{a1} \omega t \,. \tag{2.14}$$

Correspondingly, the only non-trivial equation is

$$\mathrm{d}_r^2 \rho + \frac{2}{r} \mathrm{d}_r \rho + \rho \left[\omega^2 - \alpha(\rho - f)(2\rho - f)\right] = 0 \,. \tag{2.15}$$

This has a solution that interpolates from $\rho(0) = f$ to $\rho(\infty) = 0$. The bubble is stable because of the conserved charge, equal to the occupation number of the Goldstone modes, N_{G}. In the thin-wall approximation,

$$\omega^2 \ll \alpha f^2 = m^2 \,, \tag{2.16}$$

the charge is given by,

$$N_{\mathrm{G}} = 2\pi\,\omega \int \mathrm{d}r \; r^2 \rho^2(r) \simeq \frac{2\pi}{3\alpha} m^2 \omega R^3 \,. \tag{2.17}$$

Conservation of this quantity ensures the bubble stability. In fact, this quantity breaks the degeneracy between the two vacua, allowing for a localized, stationary configuration provided that the negative core energy balances the positive wall energy.

In the thin-wall limit, such two distinct contributions split in a very clear way.

In the core, the profile is constant, and therefore the energy budget can be estimated by setting to zero the last term in (2.15) to obtain ρ_{max}. The corresponding energy is given by the energy splitting between the two no longer degenerate vacua multiplied by the volume of the configuration

$$E_{\text{core}} \sim -\int_{core} d^3x\, V(\rho_{max}) \sim -\omega^2 \frac{m^2}{\alpha} R^3, \tag{2.18}$$

while the wall-energy contribution comes from the kinetic term, and is integrated only in a small region of size m^{-1}:

$$E_{\text{wall}} \sim \int_{m^{-1}} dr\, r^2 (\mathrm{d}_r \rho)^2 \sim R^2 \frac{m^3}{\alpha}. \tag{2.19}$$

The total energy of the configuration therefore becomes

$$E \sim E_{\text{core}} + E_{\text{wall}} \sim \frac{m^3}{\alpha}\left(R^2 - \frac{\omega^2}{m} R^3\right), \tag{2.20}$$

which upon extremization with respect to R gives $R \sim m/\omega^2$.

Restoring the proper numerical factors, the energy, size and charge of the bubble can be rewritten as [8]

$$M_{\text{Bub}} = \frac{\omega}{\alpha} \frac{m^5}{\omega^5}\left(\frac{40\pi}{81}\right),\ R = \frac{2}{3}\frac{m}{\omega^2},\ N_{\text{G}} = \frac{1}{\alpha}\frac{m^5}{\omega^5}\left(\frac{16\pi}{81}\right). \tag{2.21}$$

All the above relations, up to order one factors, hold also in the thick-wall regime, in which we have

$$\omega \sim m \sim \frac{1}{R}\,. \tag{2.22}$$

In this limit, the above equations become extremely similar to the ones discussed in the previous chapter

$$M_{\text{Bub}} \simeq \frac{\omega}{\alpha},\ R = \frac{1}{\omega},\ N_{\text{G}} \simeq \frac{1}{\alpha}, \tag{2.23}$$

At this point, the characteristics of the saturon bubble of the $SU(N)$ theory become isomorphic to an equal-radius black hole of gravity, under the mapping $f \to M_{\text{P}}$. In particular, the entropy of the bubble becomes

$$S \sim \frac{1}{\alpha} \sim (Rf)^2 \sim \frac{M_{\text{Bub}}^2}{f^2}\,. \tag{2.24}$$

The source of the bubble's microstate entropy, which matches the Bekenstein-Hawking entropy of the corresponding black hole, is the exponential degeneracy of the Goldstone vacuum in the bubble interior. This is given by the combinatorics of $N_{\rm G}$ chosen from the $N-$flavour sectors of broken symmetry, providing a degeneracy and an entropy

$$n_{\rm states} \simeq \left(1+\frac{2N}{N_{\rm G}}\right)^{N_{\rm G}} \left(1+\frac{N_{\rm G}}{2N}\right)^{N}, \quad S = \log n_{\rm states}, \tag{2.25}$$

where Stirling's formula was used. In particular, to obtain (2.24), $N_{\rm G} \sim N$ is necessary. This is equivalently stated as unitarity of collective couplings $\lambda_c \simeq \lambda_t \simeq 1$. Notice how this saturation conditions, derived in the Invitation for the case of an energetic lump, are a consequence of unitarity saturation also for the non-topological soliton discussed in this Chapter.

Vorticity

In order to establish the basis for vorticity, let us notice that the Lagrangian (2.13) admits a second, topologically non-trivial, configuration in form of a global vortex line [25]. In spherical coordinates (r, φ, θ) (φ polar angle, θ azimuthal angle) it is described by the ansatz

$$\rho = \rho(r,\theta)\,, \ \chi^a = \delta^{a1} n\varphi\,, \tag{2.26}$$

where $\rho(r)$ is interpolating between $\rho(0) = 0$ and $\rho(\infty) = f$. The existence of the solution is guaranteed by the topologically non-trivial boundary condition with winding number n. The core of the vortex has a size $\delta_{\rm v} \sim 1/m$ which is comparable to the thickness of the bubble wall in the previous example.

Now, we wish to focus on a hybrid configuration in which the vortex line is piercing through a finite radius bubble. In spherical coordinates, the ansatz for the Goldstone mode describing such a configuration is

$$\rho = \rho(r,\theta), \quad \chi^a = \delta^{a1}\left(n\varphi + \omega t\right)\,. \tag{2.27}$$

The time-dependence of the Goldstone field guarantees stability of the bubble, whereas the winding number n maintains the vortex within. The resulting equation of motion is

$$\mathrm{d}_r^2\rho + \frac{2}{r}\mathrm{d}_r\rho + \frac{1}{r^2}\mathrm{d}_\theta^2\rho + \frac{\cos\theta}{r^2\sin\theta}\mathrm{d}_\theta\rho - \frac{n^2}{r^2\sin\theta^2}\rho + \rho\left[\omega^2 - \alpha(\rho-f)(2\rho-f)\right] = 0\,. \tag{2.28}$$

The above Eq. (2.28) can be solved numerically imposing the following boundary conditions [1]:

$$\rho(0,\theta) = \rho(\infty,\theta) = \rho(r,0) = 0, \quad \mathrm{d}_\theta\rho(r,\pi/2) = 0 \tag{2.29}$$

The last condition select parity-even solutions, while for $\rho(r,\pi/2) = 0$ parity-odd solution would be found.

[1]To find a numerical solution, firstly a redefinition of the radial variable was performed $R = r/(r+1)$. The solution was then found on a rectangular grid in (R,θ), employing a fourth-order finite difference scheme with an iterative Ralphson-Newton algorithm which is described in the Appendix. This was developed in C + + by the author. A similar method is used to treat Boson-stars with vorticity in [26], based on the Fortran library FIDISOL/CADSOL. A suitable initial ansatz for the profile, compatible with the boundary conditions, should be chosen in order for the iterative method to converge towards the actual solution.

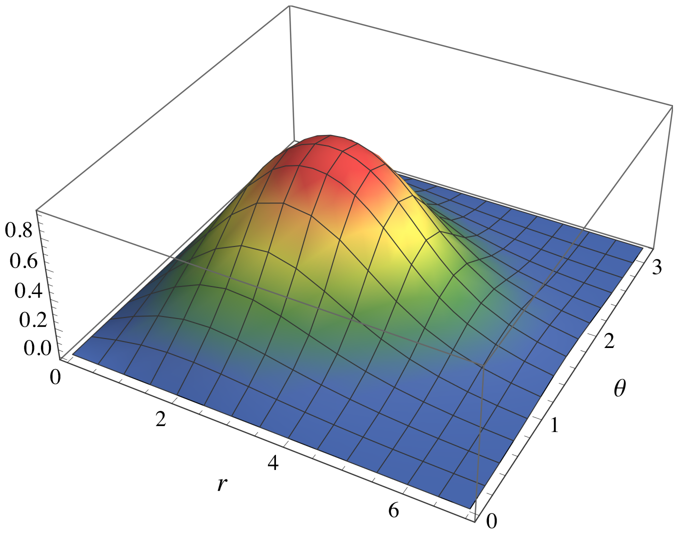

Figure 2.1: Spatial profile of axially-symmetric parity-even Q-ball with $n = 1$ vorticity.

An explicit realization of the former case is shown, for winding $n = 1$, in Fig. 2.1. While an in-depth exploration of the properties of the solution is out of the scope of this work, the found solution serves as a further proof of the existence of the discussed configurations.

As it is clear from Eqs. (2.16, 2.21), in the thin-wall limit, the radius of the bubble is much larger than the core of the vortex as well as the thickness of the bubble wall, $R \gg \delta_{\rm v} \sim \delta_{\rm w} \sim 1/m$. In the thickness-wall limit, these quantities becomes comparable.

The above winding configuration endows the bubble with angular momentum

$$J = \int T_{0\varphi} \mathrm{d}^3 x = n N_{\rm G}, \tag{2.30}$$

where, in obvious notation, $T_{0\varphi}$ denotes the relevant component of the energy momentum tensor of the system. This is very similar to the case of a spinning Q-ball considered in Ref. [27] for 2+1 dimensions and generalized to 3+1 in Ref. [28]. The important difference is that for a saturated bubble $N_{\rm G}$ is also equal to entropy. Therefore, for such a bubble we have

$$J = n N_{\rm G} \sim n S \,. \tag{2.31}$$

Notice that for the saturon bubble, the total vorticity n cannot be much higher than one. In the opposite case, the vortex energy $\sim n^2/(\alpha R)$ would exceed the entire mass of the bubble, which is impossible. This imposes the upper bound $n \sim 1$. Thus, we learn that the maximal angular momentum of the saturon bubble is

$$J_{\rm max} \sim \frac{M_{\rm Bub}^2}{f^2} \sim S \,. \tag{2.32}$$

Strikingly, this expression is similar to the one satisfied by the maximal angular momentum of a spinning black hole,

$$J_{\max} \sim \frac{M_{\mathrm{BH}}^2}{M_{\mathrm{P}}^2} \sim S\,. \tag{2.33}$$

The above similarity is remarkable in two ways. First, it gives yet another supporting evidence to the correspondence between the generic saturons and black holes. Secondly, it offers a microscopic explanation of the bound (2.33): the maximal angular momentum of a black hole is restricted by the vorticity of the graviton condensate. In addition, there can exist non-stationary non-axisymmetric configurations with zero vorticity, such as, e.g., a vacuum bubble or a black hole pierced through by multiple vortex lines with zero total winding number and unrelated spin (for a sketch see Fig. 2.2).

It should be made clear that we are not suggesting that a black hole cannot spin without vorticity. This is already clear from the fact that for a large black hole the angular moment can change almost continuously, whereas the vorticity is defined by a topological winding number. However, our point is that the maximal spin of a black hole is necessarily correlated with maximal vorticity that black hole can sustain. In this way, we provide a topological meaning to extremality. Of course, some non-stationary black holes, can carry vortices even if the total spin is zero. But such configurations will evolve in time even classically. Thus, a necessary correlation between vorticity and spin takes place only for highly spinning black holes.

Notice that as a very interesting byproduct, our picture offers a microscopic explanation for the zero temperature of extremal black holes. Thus, an extremal black hole in our picture is a black hole that has a maximal possible spin for a given mass. It is obvious that such objects cannot evaporate. Evaporation is a process that leads to a gradual decrease of the mass. Since the spectrum is thermal, emission of a quantum of arbitrarily low energy is possible. But for a black hole of maximal vorticity, such a process is not possible since the winding number cannot change continuously due to its topological nature. Our picture thus gives a topological meaning to the stability of extremal black holes. Notice that small corrections to thermality due to finite N cannot change this conclusion, since the jump in winding number requires the change of energy of order one in units of a black hole mass. Such a process has an exponentially suppressed probability and vanishes in strict semi-classical limit which represents the correct reference point for comparison with known properties of extremal black holes.

It is worth pointing out that, the degeneracy of the Goldstone vacuum, that is responsible for maximal microstate entropy, is in one-to-one correspondence with the degeneracy of the vortex configurations. This is because the vortexes are formed by the same broken generators that account for the bubble degeneracy. This connection between vorticity and the microstate entropy gives an additional basis for our proposal that analogous vorticity must be supported by black holes.

2.3 Magnetic field trapping

Despite the fact that the order parameter responsible for the vortex carries no gauge charge when interacting with some charged matter, the vortex will trap the flux of the corresponding magnetic field. This is a very general phenomenon of trapping the gauge flux by a global vortex [29], which we shall apply to the present case.

Let us represent the vortex field in form of a complex order parameter $\psi \equiv \rho \mathrm{e}^{i\theta}$. This field carries no gauge charge. Let us assume that the vortex order parameter interacts non-trivially with some fields, $\chi_+ = \rho_+ \mathrm{e}^{i\theta_+}$ and $\chi_- = \rho_- \mathrm{e}^{i\theta_-}$, carrying opposite charges $= \pm q$ under some gauge $U(1)_{\rm gauge}$ symmetry. Its rôle can be played by ordinary electromagnetism, the weak isospin, or some hidden sector symmetry. For example, these two fields can impersonate the two oppositely-charged components (e.g., electrons and ions) of the neutral plasma interacting with a black hole or a Q-ball.

Correspondingly, we assign the non-zero expectation values, $\langle\rho_-\rangle^2$, $\langle\rho_-\rangle^2 \neq 0$, which measure the properly-weighted number densities of particles. The interaction term must respect both the global shift symmetry, $\theta \to \theta + \alpha$ by a constant phase α, as well as, the $U(1)_{\rm gauge}$ gauge symmetry. Without loss of generality, we can consider the following interaction in an effective many-body Lagrangian,

$$\psi \chi_- \chi_+ + \text{h.c.} = 2\rho\rho_+\rho_- \cos(\theta + \theta_+ + \theta_-)\,. \tag{2.34}$$

This fixes the transformation properties under the global shift symmetry as $\chi_\pm \to \chi_\pm \mathrm{e}^{i\alpha}$. This transformation is orthogonal to $U(1)_{\rm gauge}$. Despite this, the vortex is trapping the magnetic field.

We can prove this by following the steps of Ref. [29]. Let us analyse the field configuration far away from the vortex core. Assuming that the electromagnetic field strength is zero, the equation for the photon field reads

$$A_\mu = \frac{1}{eq} \frac{\langle\rho_+\rangle^2 \partial_\mu \theta_+ - \langle\rho_-\rangle^2 \partial_\mu \theta_-}{\langle\rho_-\rangle^2 + \langle\rho_+\rangle^2}\,, \tag{2.35}$$

where e is the gauge coupling. Integrating the above expression over a closed path around the vortex and using Stoke's theorem, we obtain the following magnetic flux conducted by the vortex,

$$\text{Flux} = \oint \mathrm{d}x^\mu A_\mu = \frac{2\pi}{eq}\left[n_+ + n\frac{\langle\rho_-\rangle^2}{\langle\rho_-\rangle^2 + \langle\rho_+\rangle^2}\right], \tag{2.36}$$

where $n_\pm = \frac{1}{2\pi}\oint \mathrm{d}x^\mu \partial_\mu \theta_\pm$ are integers and we took into account that, regardless of the coefficient of the interaction energy (2.34), its minimization demands $n_+ + n_- = -n$. This is non-zero, unless the expectation values are adjusted to n via extreme fine-tuning, which cannot happen throughout the accretion process. In particular, for $n = 1$ such an adjustment is simply impossible.

Despite being formed by an electrically neutral order parameter, when interacting with a neutral medium with dynamical charged components, the vortex generically traps the

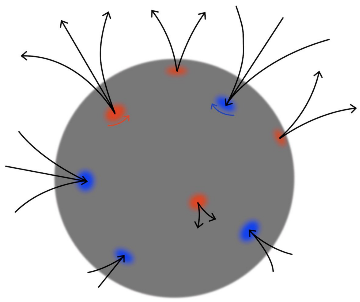

Figure 2.2: Sketch of a black hole with a number of randomly oriented vortex/anti-vortex pairs.

magnetic flux. Notice, this trapping is very different from the magnetic flux supported by Abrikosov (or Nielsen-Olesen) vortex lines in superconductors. In these cases, the primary order parameter transforms under the gauge $U(1)_{\text{gauge}}$. Due to this, the flux is quantized in units of $1/(eq)$. In contrast, the magnetic flux (2.36) trapped by a global vortex is fractional [29].

The configuration of a black hole with a trapped magnetic flux is similar to a classical solution of a black hole pierced by a cosmic string. Such solutions are well known (c.f. Ref. [30]). In the case of electromagnetic $U(1)$, the role of the flux is played by an ordinary magnetic field trapped in form of a vortex line.

In addition, the magnetic flux can have a stabilising effect against unwinding of a vortex in a way similar to how the gauge flux stabilizes the vortexes in theories with topologically-trivial vacuum structure [31]. This effect can be explicitly traced in the present case of a saturon with the vortex with fractional magnetic flux. Thus, astrophysical black holes are expected to exhibit vortex structure with the magnetic flux lines piercing through them.

2.4 Consequences of vorticity

It is well known that highly-rotating black holes can emit very powerful jets and in turn spin down (see Ref. [32] for a recent review). One important mechanism powering these jets has been suggested by Blandford & Znajek (BZ) [33]. The core idea relies on the presence of a black hole magnetosphere, which by rotation winds up in the toroidal direction and thereby leads to emission of powerful jets. For these to be sustained, the usual assumption is the presence of magnetized accreting matter around the black hole. However, for the BZ mechanism to work, the conditions concerning strength, length scale and configuration of the magnetic field must be chosen properly. Furthermore, magneto-rotational instabilities provide another complication [32].

Our proposal provides a very different framework for understanding this dynamics. As discussed in the previous section, vortexes trap the magnetic field by interacting with the surrounding neutral plasma of either ordinary or a weakly-charged dark matter. Therefore, highly-rotating black holes, can efficiently slow down due to the emission process introduced in Ref. [33]. Their total emitted power can be estimated as $P_{\rm BZ} \sim {\rm Flux}^2\Omega^2$.

Of course, the coherence of the resulting jets highly depends on the geometrical distribution of the magnetic flux. Assuming the simplest alignment with the rotational axis, the emitted power can span several orders of magnitude within the range of observational interest. Note that the maximal magnetic field (of arbitrary gauge group) that a black hole can sustain is $B \sim {\rm Flux}/R_{\rm g}^2 \lesssim M_{\rm P} R_{\rm g}^{-1} \sim M_{\rm P}^2/\sqrt{N_{\rm gr}}$.

One of the intriguing examples is the jet power observed in M87, $P_{\rm M87} \sim 10^{42\div 44}\,{\rm erg\,s^{-1}}$ [34]. The numerical simulations within the standard framework seem not to provide jets powerful enough to be compatible with the high end of the above interval [34].[2] Within our framework, the effect can potentially be accounted solely by the BZ mechanism due to vorticity.

In particular, the flux (2.36) can be macroscopic if the charge q is extremely small. For example, in case of ordinary electrodynamics, particles with very small q can be present in the form of a fluid of dark matter or even a stationary vacuum condensate.

For example, a light cold dark matter particle of mass $m_{\rm DM}$ and local energy density $\rho_{\rm local}$ in the black hole vicinity, would generate the following effective mass for the photon, $m_\gamma = eq\sqrt{\rho_{\rm local}}/m_{\rm DM}$. For illustration, let us choose both Compton wavelengths to be comparable with the gravitational radius of M87-type black hole, $m_\gamma \sim m_{\rm DM} \sim 10^{-18}\,{\rm eV}$. This in particular will guarantee the localization of the entire magnetic flux within the black hole neighbourhood. Then, for $eq \sim 10^{-39}$, (implying $\rho_{\rm local} \sim 10^4\,{\rm eV}^4$) the black hole would be endowed with a jet power compatible with observations.

In general, a constraint to be taken into account comes from the Galactic magnetic field $B_{\rm galaxy}$. In fact, due to the vorticity of the latter, the photon mass on galactic scales is bounded by $m_\gamma < \sqrt{eq\,B_{\rm galaxy}}$ [35].

The above discussion shows how the black hole vorticity could provide a "portal" into the sector of dark matter with minuscule electric charges. Curiously, in the previous example, the mass $m_{\rm DM}$ is not too far from the range of so-called "fuzzy" dark matter [36, 37]. However, at the level of the present discussion we are not attempting to establish a specific connection.

A further implication of the presence of vortexes is their impact on the evaporation dynamics of a near-extremal black hole. Due to Hawking emission these objects are expected to become extremal, at which point, as discussed previously, evaporation stops. The astrophysical consequences of this will be explored elsewhere.

Another consequence of vorticity is related to mergers of compact bodies with at least one being in the mass range around a solar mass. These are generally believed to involve neutron stars. However, as gravitational-wave observatories are not yet sensitive enough to sufficiently resolve the information on the compactness of these objects, their classification is merely by mass, plus a possible electromagnetic counterpart [38]. While the former can

[2] Note that an accretion disk might influence the BZ emission.

be accounted for by a primordial nature of the hole, the latter could be explained by its vorticity.

Chapter 3

Primordial black holes from confinement

This chapter focuses on Ref. [39], where G. Dvali, F. Kühnel and myself proposed a novel mechanism for the formation of primordial BHs (PBHs). Therein, heavy quarks of a confining gauge theory produced by de Sitter fluctuations are pushed apart by inflation and get confined after horizon re-entry. In this case, by quarks we mean any object on which flux tubes of "colour" can terminate. BH formation is due to the large amount of energy stored in the flux tube connecting the quarks pair. The resulting hole can be much lighter, and can posses an higher spin that those produced by standard collapse of horizon-size overdensities. Compared to them, no specific tuning of the inflationary potential is needed in order to obtain an abundance of PBHs comparable to an order-one fraction of dark matter. Namely, this scenario can work with arbitrary inflationary scenario. Moreover, other difficulties exhibited by such mechanisms are also avoided. Phenomenological features of the new mechanism are discussed as well as accounting for both the entirety of the dark matter and the supermassive black holes in the galactic centres. Under proper conditions, the mechanism can be realised in a generic confinement theory, including ordinary QCD. A possible string-theoretic realisation via D-branes. will also be discussed. Interestingly, for conservative values of the string scale, the produced gravity waves are within the range of recent NANOGrav data. Simple generalisations of the mechanism allow for the existence of a significant scalar component of gravity waves with distinct observational signatures.

Before plunging into discussion of the work in [39], a qualitative schematic summary of the mechanism is shown below in order to provide a clear physical picture of the mechanism.

The formation mechanism can be divided into three main steps (for simplicity focus here will be simply on a single quark/anti-quark pair):

- Inflationary fluctuations produces quarks which are diluted by the inflationary expansion as shown in the figure below.

  By the end of inflation their distance has grown as $d \propto e^{N_{\rm e}}$, $N_{\rm e}$ being the number of e-folds from the formation time until the end of inflation.

Figure 3.1

- Quarks are later confined at energy scale Λ_c.

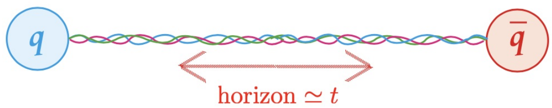

Figure 3.2

Coloured flux tubes (strings) connected to quarks form. However their collapse cannot take place due to causality as the distance between quarks is bigger than the horizon. In this period, up to the formation of a primordial black holes, $\Lambda_c < m_q$, namely, all the quarks masses should be bigger than the confinement scale in order to prevent string tunnelling into quarks pairs, therefore shortening the typical length of the string. This is the main assumption necessary for the mechanism to work. However, it does not to be fulfilled after black hole formation.

- Eventually quarks enter in causal contact, and due to the large energy stored in the string connecting them they start accelerating relativistically towards each others. The configuration Schwarzschild radius is given by

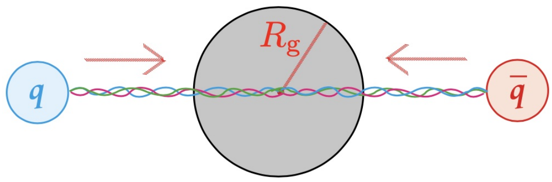

Figure 3.3

$$R_{\rm PBH} \simeq l_{\rm pl}^2 \Lambda_c^2 \, t \gg \Lambda_c^{-1} \tag{3.1}$$

Therefore the system eventually finds itself within its Schwarzschild radius, and a PBH forms.

The phenomenological consequences of the mechanism are the following:

- 100% of dark matter at $M_{\rm PBH} \sim 10^{17}$g can be obtained.

- The fraction of PBH to dark matter scales, in radiation dominated epoch, as

$$f_{\mathrm{PBH}} = \frac{\Omega_{\mathrm{PBH}}}{\Omega_{\mathrm{CDM}}} \propto M_{\mathrm{PBH}}^{-1/2}. \tag{3.2}$$

  This peculiar scaling can provide the necessary seeds to explain the observed supermassive BHs in the galactic centres.

- Depending on the confining scales, BHs lighter than the solar mass can be highly spinning due to the presence of an impact parameter induced by string-deviations from a complete straightness.

- The mechanism is compatible with known QCD if during the formation epoch

$$\Lambda_{\mathrm{c}} \lesssim m_{\mathrm{q}}. \tag{3.3}$$

  This could be realized in the Early Universe, as the expectation values of fields can change (even easier when considering moduli in string theory) before relaxing to their known temperature $T = 0$ values.

- The formation dynamics produce a unique gravitational wave signal, in particular Ω_{GW} is flat, which could be phenomenologically interesting for NANOGrav data, but also for LISA future measurements.

- A simple generalization of the mechanism can lead to the production of low-multiple gravitational contribution, which is currently not excluded by NANOGrav data.

- The mechanism is ready-made for a straightforward string-theoretic motivated implementation.

The rest of the chapter elucidates quantitatively on the above-listed points.

3.1 Introduction

Interest in black-holes has been recently fostered due to the milestone detection of mergers by LIGO/Virgo [40], together with several other events [41]. Whether these black holes could have a primordial origin is a natural question, as more of these merging objects are being detected within mass ranges at the boundary or even outside of what can be expected from stellar collapse.

Several formation mechanisms for primordial black holes (PBHs) exist on the market. The mostly focused ones, require large overdensity, which, if above a critical threshold, collapse to black holes. In most of cases, there overdensities have an inflationary origin, and collapse to PBHs upon Hubble horizon re-entry of the associated scale. Other non-inflationary scenarios for PBHs formation are based, for instance, on inhomogeneities arising from first-order phase transitions, bubble collisions, and the collapse of cosmic strings, necklaces, domain walls or non-standard vacua (see Ref. [42] for references). Despite the existence of several attempts, finding a viable mechanism for the production of PBHs remains a challenging question for both cosmology and particle physics.

In this Chapter a novel mechanism for the productions of PBHs is presented, which is rather natural within the framework of confining theories, such as, asymptotically-free QCD-like gauge theories with massive quarks. This mechanism is based on the dilution of heavy quarks produced during inflation which get confined by QCD-like flux tubes upon horizon re-entry. PBH formation is then caused by the large amount of energy which is stored in the string connecting the quark pairs. A similar mechanism was proposed in [43], where black holes are formed via the collapse of monopoles connected by cosmic strings. Differently from it, quarks can be produced as perturbative states during inflation. On top of that, the asymptotic freedom of the theory, guarantees their confinement by QCD flux tubes. Consequently the proposed mechanism can be implemented also within the Standard Model QCD, under proper conditions during during the Early Universe, which will be specified later

We also speculate about the string-theoretic realisations of this mechanism. In this case, the rôle of heavy quarks is played by compact D-branes produced by de Sitter fluctuations during brane inflation. The rôle of the QCD flux tubes connecting them are played by D-strings which form after graceful exit. We estimate that for conservative values of string-theoretic parameters, the gravitational waves produced during the confinement process is in interesting range for NANOGrav data [44].

A scalar component of the emitted gravitational waves from PBH formation can follow from a simple generalization of our scenario, potentially leading to interesting observational signature such as the existence of low multiple as well as the dependence of detected power of the gravity waves on the isotope composition of the detector. In fact, as pointed by NANOGrav observations, given the current observational sensitivity, further non-quadrupolar contribution to the signal is not yet excluded. Future verification of this possibility, could provide a hint of such a non-standard gravitational-wave contributions.

This chapter is structured as follows.The mechanism and its dynamics are described in Sec. 3.2. The cosmological relevance for the production of PBH dark matter, as well as for supermassive black holes in galactic centres ias addressed in Sec. 3.3. Here the viability of the scenario within QCD as well as in string-theoretic context is addressed together with the above-mentioned generalization necessary to obtain a scalar component of emitted gravitational waves from PBH formation. The last section 3.4 is left for Discussion and Outlook

Throughout this chapter units in which $M_{\rm P} = c = \hbar = 1$, unless explicitly stated for clarity, are used.

3.2 Mechanism

A QCD-like gauge theory with massive quarks is the key ingredient of our scenario. By "quark" it is meant a generally arbitrary "coloured" state onto which the associated gauge flux tube can end. Throughout the formation epoch, quarks must be heavier than the associated confinement scale, Λ_c, in order to ensure the string non-fragmentation; a necessary condition for the scenario to work. This epoch covers from the last 60 or so e-folds of the inflationary period, up to the radiation/matter domination era, during which the black holes are formed. Afterwards, the relation between quark masses and Λ_c can change, even reverse, with quarks lighter than the confining scale. Such change will not affect the outcome of PBH formation. Since, generically the expectation values of the fields change throughout cosmology, the class of possibility is rather wide and can include even "our" QCD.

In the simplest scenario it can be assumed that during the inflationary period QCD was not confining i.e., that the confining scale $\Lambda_c < H_i$ at that time, where H_i denotes the inflationary Hubble. In this case, de Sitter fluctuations will produce quark/anti-quarks which will be freely inflated afterwards.

In the opposite case ($\Lambda_c > H_i$), from the moment of their formation quarks will be connects to a QCD flux tubes, which, in turn, causes a suppressed nucleation probability due to the additional contribution from the flux tube.

The proposed scenario then works as follows: consider a quark/anti-quark pair, exponentially diluted by the inflationary expansion to distances much bigger than the inflationary horizon. Eventually the pair comes in causal contact during the later radiation dominated era, when it gets confined by strings of tension $\mu = \Lambda_c^2$. In this case the energy stored in the confining string, and in the system (the monopole mass is negligible compared to these horizon size strings), is

$$E \sim \Lambda_c^2 \, t \,, \tag{3.4}$$

where t is the time of horizon re-entry of the pair.

Once within causal contact, the two quarks start moving towards each other with acceleration proportional to Λ_c^2/m_q, becoming quickly ultra-relativistic. Due to the large amount of energy stored in the confining string, the system's Schwarzschild radius $R_g \sim E$ is much bigger than the string width Λ_c^{-1}. This implies the condition

$$\frac{\Lambda_c^2}{\sqrt{g_*(T)}\, T^2} \gg \frac{1}{\Lambda_c} \,, \tag{3.5}$$

which results in the formation of a PBH of mass $M_{\rm PBH}$,

$$M_{\rm PBH}(t) \sim E(t) \sim \Lambda_c^2 \, t \gg \Lambda_c^{-1} \,. \tag{3.6}$$

Eq. (3.6) can readily be expressed in terms of the temperature T at the time of formation:

$$M_{\rm PBH}(T) \approx \frac{3\sqrt{5}\, \Lambda_c^2}{4\pi^{3/2}\sqrt{g_*(T)}\; T^2} \,. \tag{3.7}$$

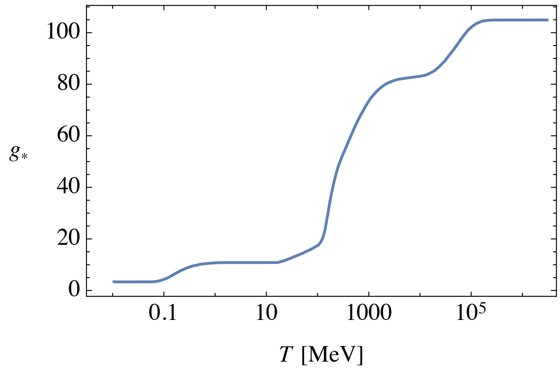

Figure 3.4: Number of relativistic degrees of freedom as a function of temperature (adopted from Ref. [45]).

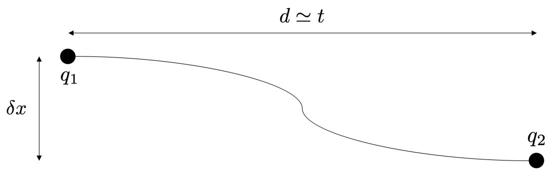

Figure 3.5: Sketch of the initial configuration at collapse, for which $\delta x \ll d$.

Where, $g_*(T)$ is the number of relativistic degrees of freedom at temperature T (depicted in Fig. 3.4).

The PBH mass in Eq. (3.6) should be compared with the one obtained from the collapse of horizon-size overdensities [46, 47, 48], in which case we have

$$\widetilde{M}_{\rm PBH}(t) \approx \gamma\, t \,, \tag{3.8}$$

with $\gamma \sim \mathcal{O}(1)$.[1] Hence, $\widetilde{M}_{\rm PBH}$ is much larger than that of our proposed mechanism; their ratio being

$$\frac{M_{\rm PBH}}{\widetilde{M}_{\rm PBH}} \approx \frac{\Lambda_{\rm c}^2}{\gamma} \ll 1 \,. \tag{3.9}$$

Before discussing the conditions necessary to obtain 100% of PBH dark matter, the spin of the resulting black holes is addressed in the next Section.

Spin

Duuring the inflationary period, de Sitter quantum fluctuations, induce a Brownian motion of the string zero mode, related to the string straightness. This is of order $H_{\rm i}$ for each

[1]Here, for simplicity, we neglect the effect of critical collapse (c.f. Refs. [49, 50, 51, 52, 53, 54, 55]), which leads to a PBH mass spectrum.

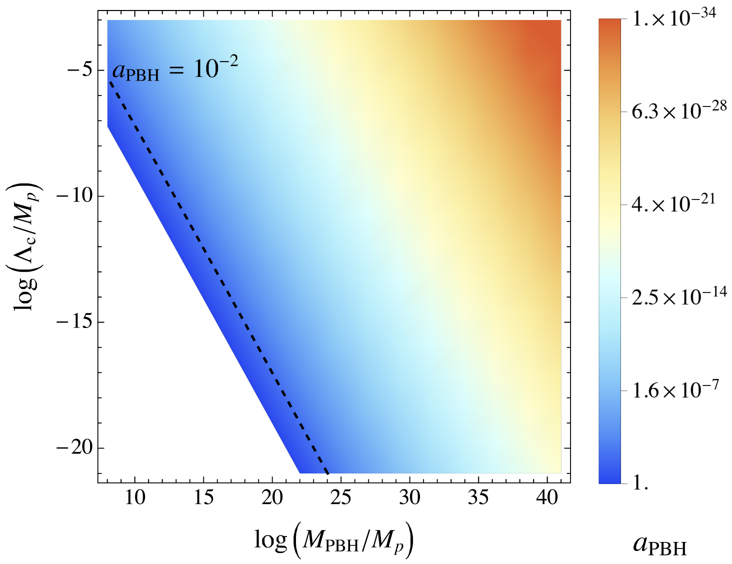

Figure 3.6: Dimensionless spin $a_{\rm PBH}$ at formation time as a function of $M_{\rm PBH}$ and $\Lambda_{\rm c}$ according to Eq. (3.12). The case $\Lambda_{\rm c} \gtrsim H_{\rm i}$ is considered.

Hubble time $H_{\rm i}^{-1}$, leading to the following estimate on the string non-straightness

$$\delta x \simeq \sqrt{N_{\rm e}}\, H_{\rm i}^{-1} \,, \tag{3.10}$$

$N_{\rm e}$ being the number of e-folds from the string-pair nucleation time to the end of inflation, and is given by

$$N_{\rm e} = \frac{1}{2}\log\left(\frac{M_{\rm PBH}H_{\rm i}}{\Lambda_{\rm c}^2}\right) . \tag{3.11}$$

Eq. (3.10) serves as a good estimate for the impact parameter at black-hole formation, as the quark/anti-quark pair collapses ultra-relativistically in the radiation-dominated epoch (see Fig. 3.5 for a sketch of the initial collapsing configuration). In the following this is assumed to be the only mechanism sourcing angular momentum for PBHs. Therefore the dimensionless Kerr spin parameter $a_{\rm PBH}$ at formation is approximated by

$$a_{\rm PBH} \simeq \frac{\delta x}{R_{\rm g}} \simeq \frac{1}{H_{\rm i}M_{\rm PBH}} \log\left(\frac{H_{\rm i}\, M_{\rm PBH}}{\Lambda_{\rm c}^2}\right)^{1/2} , \tag{3.12}$$

where numerical factors of order one have been neglected.

Notice that the condition (3.5) translates into a constraint $a_{\rm PBH} < \sqrt{N_{\rm e}}\Lambda_{\rm c}/H_{\rm i}$, where $\Lambda_{\rm c}$ is the string scale during the re-entry. Therefore, special attention has to be paid to the scenarios in which this quantity changes significantly relative to its inflationary value, as this can constrain the impact parameter significantly. For the simplest case when throughout the process $\Lambda_{\rm c} \sim H_{\rm i} \sim R_{\rm g}^{-1}$, Eq. (3.12) would result into a near-maximal spin.

Equation (3.12) is depicted in Fig. 3.6, for the case $\Lambda_c \gtrsim H_i$ (logarithmic corrections are to be included if this condition is relaxed). The white region corresponds to an impact parameter bigger than the corresponding configurations's Schwarzschild radius. In this case the system is expected to undergo rotations while rotating, and requires a more accurate study, which includes also back-reaction. This is beyond the scope of this work.

Highly-rotating black holes can be produced. Especially for low mass values, but high confining scales (see Fig. 3.6). It is clearly possible to have formation of *maximally*-spinning PBHs consistent with structure-formation constraints which demand the presence of dark matter at latest around redshift $\mathcal{O}(10^4)$ corresponding to $T \sim \mathcal{O}(10)\,\mathrm{eV}$. Of course, isolated events of black-hole formation via confinement could still have taken place at much later time, and might occur even today, with potentially detectable signatures.

According to the estimate (3.12), heavier black holes will not be spinning significantly. It is known that the spin of black holes of mass $M_{\mathrm{PBH}} \sim M_{\odot} \sim 10^{38}\,M_{\mathrm{P}}$ cannot be caused by inflationary fluctuations as being clear from Fig. 3.6. However, in this region PBHs can start spinning due to accretion [56]. Other spin sources might be relevant for spin in this case, depending on the specific implementation of the mechanism.

Finally, the window between 10^4 g and 10^{10} g, as discussed in Sec. 3.3, is an interesting region in which higher inflationary scales can contribute to the PBH spin, therefore making it very attractive from an observational point of view. In general, probing PBH spins in the mass range close to the blue-coloured area of Fig. 3.6 could not only serve as a check of the proposed mechanism but also as an indirect measurement of the inflationary scale H_i.

As it is clear from the above discussion spin may be used to distinguish between PBHs which from confinement versus the standard mechanism via overdensities. While the former can give maximally-rotating black holes, $a_{\mathrm{PBH}} \sim 1$, the latter has an upper bound on the spin at formation $a_{\mathrm{PBH}}^{\mathrm{overdense}} \lesssim 10^{-1}$ as discussed in Ref. [57] (see also Refs. [58, 59], and Ref. [60] for producing larger spins in the matter-dominated era). Further accretion cannot help to significantly increase the PBH spin as long as $M_{\mathrm{PBH}} \ll M_{\odot}$ as shown by Ref. [56].

3.3 Dark Matter

In this section the question as to whether the confinement mechanism can form an order-one fraction of the dark matter is addressed. Some similarities are shared with the mechanism proposed in Refs. [61, 62], where bubble produced in the inflationary period are exponentially stretched by the cosmological expansion, and later, during radiation domination, re-collapse. Differently from it, our scenario does not require fine-tuning of the production rate of quarks during the inflationary period in order to obtain the entirety of dark matter.

The quark mass m_q can be higher or lower than the inflationary Hubble scale H_i. In the first case an exponential suppression of the nucleation takes place, similar to the dual monopole case. Indeed, heavier objects than the Hubble scale are produced due to de Sitter Gibbons-Hawking effective temperature $T_h = H_i/2\pi$

The quark mass $m_{\rm q}$ can be either higher or lower than the inflationary Hubble scale $H_{\rm i}$. In the former case nucleation processes are exponentially suppressed, similar to the dual monopole-case. In fact, objects heavier than the Hubble scale can be produced due to de Sitter Gibbons-Hawking effective temperature $T_{\rm h} = H_{\rm i}/2\pi$ [63], whose rate scales as [64]

$$\lambda \propto e^{-B} , \tag{3.13}$$

where for quarks $B = m_{\rm q}/T_{\rm h} \equiv B_{\rm q}$ (see Ref. [64]). The QCD confininng scale can be either below or above the inflationary Hubble. In the latter case, quarks are already in a confined phase, and also the string nucleation probability contributes to Eq. (3.13), namely $B = B_{\rm q} + 2\Lambda_{\rm c}^2 R_{\rm s}/T_{\rm h}$, where $R_{\rm s}$ corresponds to the string length. Taking string-gravity effects into account, leaves the exponential suppression unaltered as shown in [64]. Moreover it is needed

$$\Lambda_{\rm c} \lesssim m_{\rm q} \tag{3.14}$$

which suppress the tunnelling probability of cosmologically long strings into quarks-pairs upon horizon re-entry later in the Universe history. Note that this probability per unit-length, per unit-time is given by $P \propto \exp(-\pi\, m_{\rm q}^2/\Lambda_{\rm c}^2)$ (see Ref. [25]).

Since Eq. (3.13) follows from a semi-classical calculation, it holds trues for $m_{\rm q}$ (and if confined during inflation, the confinement scale $\Lambda_{\rm c}$) bigger than the inflationary Hubble scale. While quarks are inflated during the inflationary period, their final density should not be too diluted, namely during the inflationary period $m_{\rm q}(\Lambda_{\rm c}) \gtrsim H_{\rm i}$ is required. It follows that the pre-factor in (3.13) is expected to be of order one.

Independently of the nucleation scenario it is possible to compute the PBH dark-matter fraction, being defined as

$$f_{\rm PBH} \equiv \frac{\rho_{\rm PBH}(t)}{\rho_{\rm CDM}(t)} = \frac{1}{\rho_{\rm CDM}(t)} \int {\rm d}M_{\rm PBH}\, \frac{{\rm d}n_{\rm PBH}(t)}{{\rm d}\ln M_{\rm PBH}} , \tag{3.15}$$

in which $\rho_{\rm CDM}$ is the energy density of cold dark matter (CDM). If the collapse takes place in a radiation-dominated universe, it can be expressed as

$$\rho_{\rm CDM}(t) \approx \frac{3}{16\pi\, t^{3/2}} \frac{1}{M_{\rm eq}^{1/2}} , \tag{3.16}$$

where $M_{\rm eq} = t_{\rm eq} = 2.8 \times 10^{17}\, M_\odot \sim 10^{55}$, corresponding to the cosmological horizon mass at the time $t_{\rm eq}$ of matter-radiation equality. The number density of PBHs redshifts in exactly the same way as $\rho_{\rm CDM}$:

$$\frac{{\rm d}n_{\rm PBH}(t)}{{\rm d}\ln M_{\rm PBH}} \approx \lambda\Lambda_{\rm c}^3\, \frac{1}{M_{\rm PBH}^{3/2}}\, \frac{1}{t^{3/2}} , \tag{3.17}$$

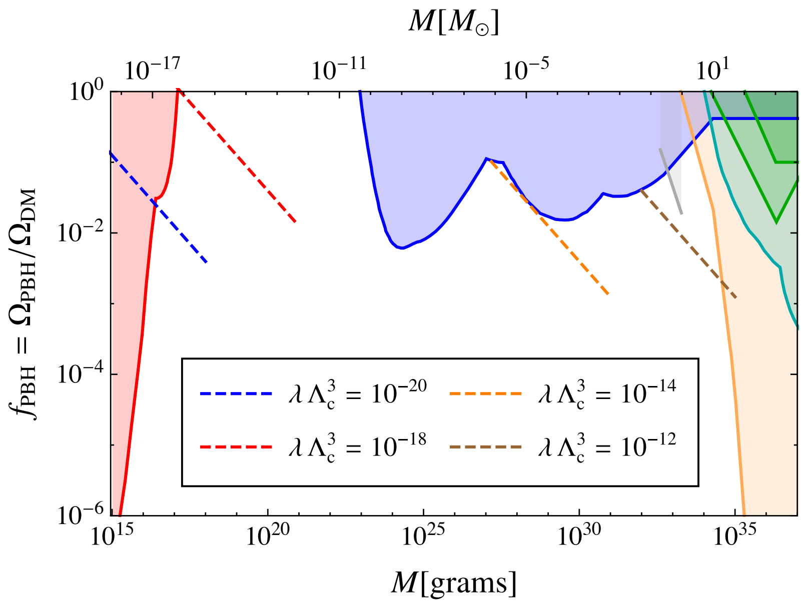

Figure 3.7: Mass dependence of $\mathrm{d}f_{\rm PBH}/\mathrm{d}\ln M_{\rm PBH}$ for different values of the combination $\lambda\Lambda_c^3$ according to Eq. (3.18). *Shaded areas*: Constraints on $f_{\rm PBH}$ for a monochromatic mass function, from evaporations (red), lensing (blue), gravitational waves (GW) (gray), dynamical effects (green), accretion (light blue), CMB distortions (orange) (see Ref. [42]).

where a constant λ given by Eq. (3.13) was assumed through inflation (as discussed below Eq. (3.13) the prefactor is of order-one). Combining Eqs. (3.16, 3.17), we find for the present PBH dark-matter fraction, Eq. (3.15),

$$f_{\rm PBH} \approx \frac{32\pi}{3}\,\lambda\Lambda_c^3 \left(\frac{M_{\rm PBH}}{M_{\rm eq}}\right)^{-1/2} . \tag{3.18}$$

For different values of the combination $\lambda\Lambda_c^3$, $\mathrm{d}f_{\rm PBH}/\mathrm{d}\ln M_{\rm PBH}$ is shown in Fig. 3.7; the shaded areas indicate the existing observational constraints on the PBH abundance (see Ref. [42]). Since these are computed for the case of a monochromatic spectrum, the fact that the dotted lines do not intersect the shaded ones, does not imply a viable realization of the scenario, but it should rather be considered only as an indication of such.

It is clear that the $M_{\rm PBH}^{-1/2}$ scaling of Eq. (3.18) leads to heavy constraints. Note that a possible cut-off in the spectrum is given by the tunneling probability $P_{\rm tunnel}$ of the string into quark/anti-quark pairs per unit-time per unit-length. This sets a critical length, for which longer strings will start to break into shorter strings configurations [25]. This can schematically be estimated as

$$P_{\rm tunnel} \propto e^{-\pi\, m_q^2/\Lambda_c^2}\ , \quad P_{\rm tunnel}\, t_{\rm crit}^2 \overset{!}{=} 1\ , \tag{3.19}$$

where in the second equation $t_{\rm crit}$ is defined. The string breakage will therefore affect PBHs in the spectrum at masses around $M_{\rm PBH} \sim \Lambda_c^2 P_{\rm tunnel}^{-1/2}$. Although in an explicit realization

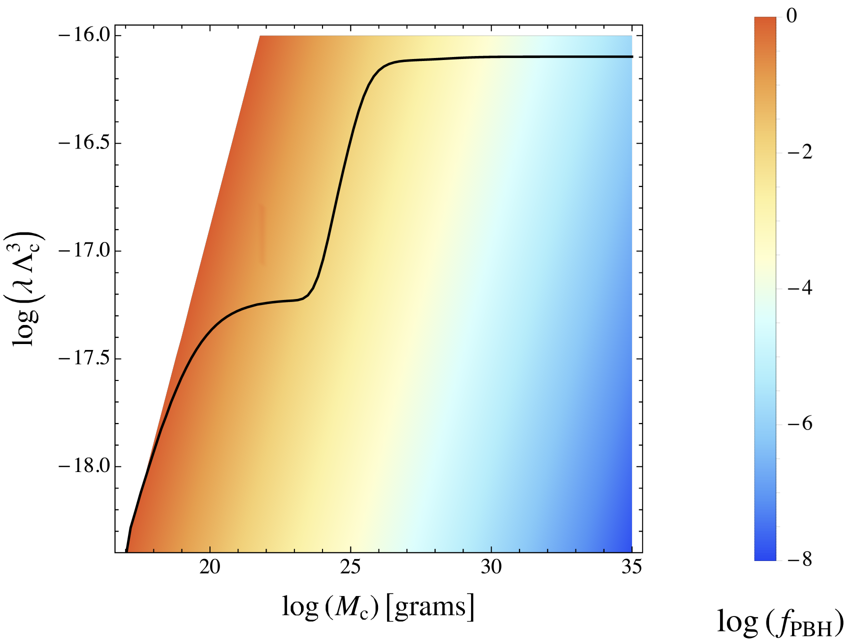

Figure 3.8: Dependence of $f_{\rm PBH}$ on the highest value of the mass-spectrum, M_c, and the combination $\lambda\Lambda_c^3$ [see Eq. (3.18)]. The black line corresponds to saturation of Eq. (3.20) below which the scenario admits PBH as dark matter.

this could be the case, given the working assumption $\Lambda_c \ll m_q$ we neglect such possibility in the following discussion, even though this could be phenomenologically relevant for certain region of the parameter space.

To check whether all of the dark matter can be accomodated with the confinement mechanism, a constraint analysis accounting for the whole extended PBH mass function was performed. Therefore we impose the condition [65]

$$\int_{M_1}^{M_2} \mathrm{d}\ln M_{\rm PBH}\, \frac{\mathrm{d}f_{\rm PBH}(M_{\rm PBH})}{\mathrm{d}\ln M_{\rm PBH}}\, \frac{1}{f_{\rm max}(M_{\rm PBH})} \overset{!}{\leq} 1\,, \tag{3.20}$$

where $f_{\rm max}(M_{\rm PBH})$ corresponds to the maximal allowed value of $f_{\rm PBH}$ in the case of a monochromatic spectrum as given in Fig. 3.7. For the analysis, we focus on the region between $M_1 = 10^{17}$ g, $M_2 = 10^{37}$ g and show our results in Fig. 3.8. M_c corresponds to the highest mass in $\mathrm{d}f_{\rm PBH}/\mathrm{d}\ln M_{\rm PBH}$. The black line is obtained by saturating the inequality in Eq. (3.20). Values below that are compatible with experimental constraints. We note that for a maximum mass M_c between 10^{17} g and 10^{19} g, corresponding to $\lambda\Lambda_c^3 \approx 10^{-18}$, the entire dark matter can be accommodated for. In order to obtain a PBH of mass 10^{17} g, the corresponding choice of $\lambda \approx 10^{-3}$ and $\Lambda_c \approx 10^{-5}$ requires $T \simeq 8 \cdot 10^{-16}$ [see Eqs. (3.6, 3.7)].

Of phenomenological relevance could also be the case where PBHs are formed during a matter-dominated epoch. This could happen while the inflaton relaxes oscillating around its minimum at the end of inflation or if the collapse takes place after equality (or in some non-standard cosmological history). In all cases, the PBH dark-matter fraction scales as

$$f_{\rm PBH}^{\rm md} \propto \ln M_{\rm PBH} \,. \tag{3.21}$$

It follows that in the case of an extended spectrum, such as the one considered in Fig. 3.8, the parameter window realising order-one fraction of dark matter is smaller for extended periods of matter domination. In general, small periods of matter domination would still make the scenario viable in several regions of the parameter space.

The scenario avoids one of the biggest issues plaguing the standard mechanism for PBH productions based on the collapse of horizon-size overdensities as it requires no exponential fine-tuning. In fact, if the PBHs form from Gaussian inhomogeneities with root-mean-square amplitude σ, then the fraction β of horizon patches undergoing collapse to PBHs is [48]

$$\beta \approx \mathrm{erfc}\left[\frac{\delta_{\rm c}}{\sqrt{2}\,\sigma}\right] , \tag{3.22}$$

where 'erfc' is the complementary error function and $\delta_{\rm c} \equiv \delta\rho_{\rm c}/\rho$ corresponds to the critical threshold for black-hole formation.[2] As it is apprent from Eq. (3.22), there is an exponential sensitivity of the PBH abundance on the amplitude of the primordial power spectrum. Differently, the mechanism based on confinement avoids this sort of exponential fine-tuning, as the resulting collapsing dynamics is (almost) uniquely determined by the system itself, and is but slightly affected by the surrounding environment. As discussed above, a phenomenological-window capable of justifying an order-one fraction of the presently observed dark matter is also easily obtained.

Supermassive Black Holes

An open questions in current astrophysics is about the origin of supermassive black holes (SMBH), i.e., those black holes with a mass higher than about $M_{\rm BH} \gtrsim 10^5\, M_\odot$. These objects are observed in the galactic centres [70]. Their origin is difficult to be justified by standard accretion of stellar black holes. In fact, accretion mechanisms become effective rather later in the universe (i.e. at redshifts between $0 \leq z \leq 6$, compatibly with Galaxy formation). However, heavy black holes with masses $M_{\rm BH} \gtrsim 10^9\, M_\odot$, are observed at earlier times ($z \gtrsim 6$) as pointed in Refs. [71, 72]. This opens the questions for their origin. The observational ratio between the mass of a galaxy, $M_{\rm galaxy}$, and that of the supermassive black holes, $M_{\rm BH}$, at its centre is approximately [70]

$$\frac{M_{\rm galaxy}}{M_{\rm BH}^{\rm centre}} \sim 10^5 \,. \tag{3.23}$$

[2]During the radiation-domination, assuming spherical collapse, a value of $\delta_{\rm c} = 0.45$ has been obtained using numerical simulations (c.f. Ref. [66]). This value depends on the shape and the statistics of the overdensities which undergo gravitational collapse (see Refs. [67, 68] for spherical perturbations and Ref. [69] for non-spherical shapes). Furthermore, there is a slight discrepancy amongst the results of various groups.

When combined with the number density of galaxies massive enough to host a SMBH [73], an amount of PBHs of order $f_{\rm PBH}^{\rm centre} \sim 10^{-7}$ is required (see Ref. [74])[3]. These super-heavy objects, due to the rather-slowly decaying mass spectrum, are a byproduct of our mechanism.

In fact, if we focus on the window where an order-one fraction of dark matter is produced via confinement, namely for a maximal mass $M_{\rm c} \sim 10^{19}\,{\rm g}$, $\lambda\Lambda_{\rm c}^3 \sim 10^{-18}$, we obtain

$$f_{\rm PBH}^{\rm heavy} \equiv \int_{10^4 M_\odot}^{M_{\rm eq}} {\rm d}\ln M_{\rm PBH}\, \frac{{\rm d}f_{\rm PBH}(M_{\rm PBH})}{{\rm d}\ln M_{\rm PBH}} \approx 10^{-10}\,. \tag{3.24}$$

The resulting value $f_{\rm PBH}^{\rm heavy}$ is essentially independent w.r.t. the upper cut-off already a few orders of magnitude above the lower one. Finally, taking into account accretion, PBHs for which $M_{\rm PBH} \gtrsim 10^4\,M_\odot$ at formation, can increase their value up to the one observed of $10^9\,M_\odot$ as seen in Ref. [75]. This accretion mechanism, however, slows down for heavier masses $M_{\rm BH} \gtrsim 10^{10}\,M_\odot$ as discussed in Ref. [76]. This process may increase $f_{\rm PBH}^{\rm heavy}$ to the necessary value of 10^{-7}, which would be in complete agreement with the recent analysis of Ref. [72]. There it is shown, via semi-analytical arguments, that PBHs of mass $M_{\rm PBH} \gtrsim 10^4\,M_\odot$, not only can accrete to the desired SMBH masses, but they can do so without conflicting with current observational bounds, justifying the current amount of observed SMBHs as long as $f_{\rm PBH}(M \gtrsim 10^4\,M_\odot) \lesssim 10^{-9}$. Direct comparison with Eq. (3.24) shows that SMBHs are a natural consequence of PBHs generated via confinement.

Evaporation Constraints

Usually, Hawking radiation [77, 78] is assumed to be valid for the entire lifetime of a black hole. Consequently, PBHs with masses below about $10^{15}\,{\rm g}$ are not considered to be viable dark-matter candidates, as they would have fully evaporated by now.

This is based on an extrapolation of the semiclassical computation, well beyond its domain of validity. Clearly, through the decay process, backreaction becomes non-negligible, latest by the time the black holes has emitted half of its original mass.

The results of [19], where back-reaction is performed in an explicit prototype model describing the microscopic structure of a black hole [19], confirms this intuition. In fact, by its half-decay, the full quantum evolution of the system departs from the semiclassical one. This is due, for example, to the back-reaction of quantum information carried by the hole [79].

Ref. [80] argued that, given the inability of a black hole to get rid efficiently of this information, Hawking radiations is slowed down, and eventually halted. The slow-down of the decay process at latest by the time of half-decay has been shown to unambigously take place in various prototype models. Even though the final fate of a black hole beyond

[3]The value of $f_{\rm PBH}^{\rm centre}$ might vary by several orders of magnitude due to uncertainties in the accretion mechanism ($f_{\rm PBH}^{\rm centre}$ could be as low as 10^{-9} as commented in Ref. [74]).

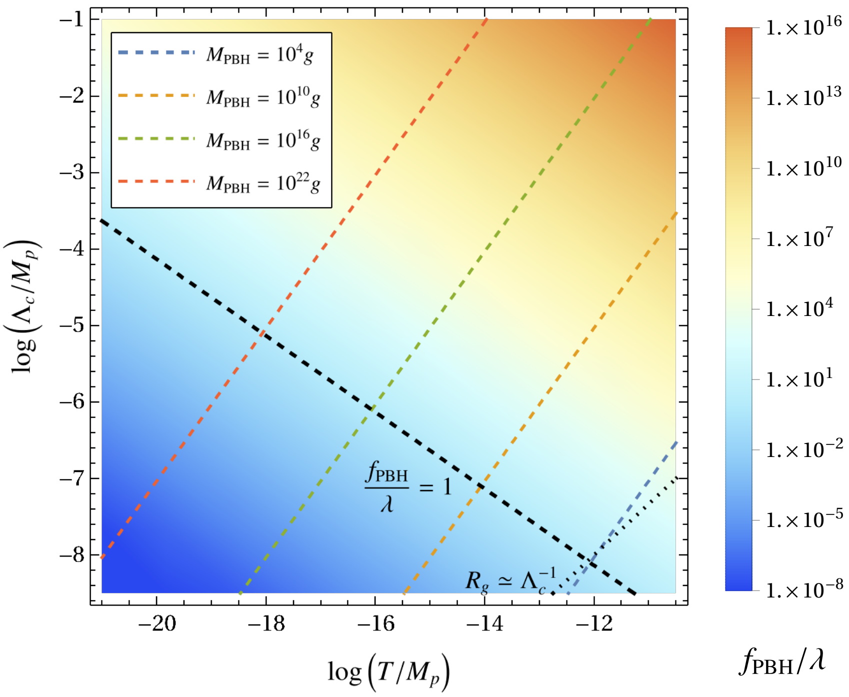

Figure 3.9: Density plot of f_{PBH}/λ vs. T and Λ_{c} according to Eq. (3.18). The dashed black line corresponds to $f_{\mathrm{PBH}}/\lambda = 1$, while the dotted black line is given by $R_{\mathrm{g}} \simeq \Lambda_{\mathrm{c}}^{-1}$.

this time requires deeper analyses, enough evidence is provided to conclude that it was premature to discard PBHs lighter than 10^{15} g from the list of dark matter candidates.

Adopting the most conservative result of Ref. [80], namely, assuming a correction to the black-hole lifetime τ of the form

$$\tau \rightarrow S^2 \tau \, , \tag{3.25}$$

with S being the BH entropy. From Eq. (3.25), it follows that BHs of masses larger than $M_{\mathrm{BH}} \geq 10^4$ g have a lifetime longer than the age of the Universe, t_0, and therefore might indeed be possible dark-matter candidates. Heavier BHs from 10^{10} g up to 10^{15} g would still be constrained from BBN and CMB, although in a weaker way as they would emit a much less intense radiation. Heavier PBHs for which $M_{\mathrm{PBH}} \geq 10^{16}$ g have unaltered constraints, given the validity of the semi-classical description throughout the age of the Universe.

In Fig. 3.9 the dependence of f_{PBH} for different values of the confining scale Λ_{c} and temperature T is shown. Between 10^4 g and 10^{10} g a 100% fraction of the dark matter could be explained by PBHs. The dotted line $R_{\mathrm{g}} \simeq \Lambda_{\mathrm{c}}^{-1}$ corresponds to the limiting case for black-hole formation, as in this case the gravitational radius becomes comparable to the thickness of the QCD string.

The case of rotation

Another stabilizing source for extremely light PBHs is vorticity. As already discussed, this scenario easily allows for the production of highly-spinning BHs, close-to-extremal. These, in turn, as argued in Chap. II, posses a vortex structure. The topological nature of the vortex, being the winding number n an integer, forbids the emission of soft-quanta emission process, such as Hawking emission. This offers yet another reason against the premature dismiss of PBH lighter than 10^{15} g as dark matter candidates.

Moreover, in the case of rotating PBHs, other phenomenological consequences follow. The vortex, which is a global order parameter, can act as a support for the magnetic field, which is induced by its interaction with mobile charges surrounding the hole. This effectively result in an effective local mass for the photon surrounding the PBH and the confinement of the associated $U(1)$ magnetic flux follows.

This mechanism can take place for any sector, and therefore it can serve as a portal to some dark sector (see discussion in Chap. II). If, however, the actual confined "magnetic" flux is the one from our electromagnetic sector, $U(1)_{\rm em}$, the resulting PBHs would effectively source also primordial magnetic fields. Later dynamo amplifications of these effect could provide an explanation for the observed galactic magnetic field. The details of this are left for future works.

Gravitational Waves

The collapse of a quark/anti-quark pair into a PBH leads to the emission of gravitational radiation. A monopole/anti-monopole system connected by a cosmic string [81] is expected to emit gravity in a similar way. Given that the size of the impact parameter matters only at BH formation, gravity waves can be estimated in the approximation of a straight QCD-string attached to quarks.

The lowest frequency produced by the collapse of a single pair corresponds to approximately its initial inverse distance: the cosmological horizon, given by the cosmological time t. As explained above, the impact parameter becomes relevant on distances comparable to the Schwarzschild radius of the configuration, while for the present focus we will look at frequencies on much longer lengths. Therefore the dynamics can be assumed to be head-on. In this case, the monopole/anti-monopole confined dynamics, which applies in this case, was studied by Ref. [81], where it was shown to lead to an emitted gravitational-wave spectrum P_n at frequency $\omega_n = 2\pi n/t$

$$P_n \sim \frac{\Lambda_{\rm c}^4}{n} \,. \tag{3.26}$$

The validity of Equation (3.26) is up to frequency numbers of order $M_{\rm PBH}^2/m_{\rm q}^2$ [81]. For higher harmonics, P_n decreases first as n^{-2}, and is eventually exponentially suppressed [81, 82, 83]. In our case, given the enormous energy stored in the string at initial times, Eq. (3.26) can be safely used through our discussion. As shown by Ref. [81] the radiated power is emitted in a small beaming angle oriented along the collapse direction; it can be estimated as $\theta \sim n^{-1/2}$ [81]. In the proposed scenario, it might be possible, in certain regions of the parameter space, to produce an observationally relevant stochastic gravitaitional-wave background.

A similar analysis was performed in Ref. [84, 85], where the gravitational-wave signal due to the rapid annihilation of monopole pairs, linked by straight strings, was studied. This was found to lead to a flat $\Omega_{\rm GW}$. Therefore, assuming the mass distribution extends to $M_{\rm PBH} \gg \Lambda_{\rm c}^2 f^{-1}$, f being the gravitational-wave frequency, the resulting spectrum is nearly scale invariant.

This could be relevant in view of the recent NANOGrav date, found at a frequency $f = \text{year}^{-1}$. This is easily mapped to a formation time within the confinement scenario around 10^{-3} s. Refs. [84, 86, 85] can be followed to estimate the resulting gravitational-wave background from confinement, giving

$$\Omega_{\rm GW}^{\rm NANO} \sim 10^{-11} \propto \lambda \Lambda_{\rm c}^4 \, . \tag{3.27}$$

The pre-factor depends slightly on the extension of the PBH spectrum distribution. It is of $\mathcal{O}(1)$ if PBHs are still forming today. This implies $\Lambda_{\rm c} \geq 10^{-2.5}$ to match observations. Indeed a lower scale would suppress the amount of emitted gravitational waves too much. It is interesting to note that the amplitude of NANOGrav data (3.27), for a gravitational flat signal, would be within the prospective reach of LISA [85].

We would like to point out that a mild extension of our scenario can provide a significant (or even a dominant) scalar component of gravity waves. This would be the case if there would exist a massless scalar field interacting both with heavy quarks as well as with the Standard Model particles. For example, it suffices to couple the mediator scalar to the heavy quarks via a standard Yukawa interaction with coupling constant g.

In order to have an interesting observable effect, this coupling must be stronger than gravity. Let us parameterise by ϵ the relative strength of the effective coupling of the scalar to the Standard Model particles with respect to gravity. This quantity must be very small in order to accommodate phenomenological constraints on gravity-competing forces. In particular, the equivalence-principle violating part of such interaction must obey $\epsilon \lesssim 10^{-6}$ [87, 88]. In case of an equivalence-preserving interaction, the constraints are milder, $\epsilon \lesssim 10^{-3}$ or so [89].

Under such circumstances the power of the scalar gravitational radiation relative to a tensor one, as seen by a detector constructed out of ordinary Standard Model matter, is controlled by the product $g\epsilon$. At the expense of having large g, this parameter can be within the range of observational interest, even for the values of ϵ well within the above phenomenological bounds. This provides an interesting motivation for the search of gravitational waves with rather unusual properties. In particular, such waves can carry a scalar monopole component and their observed intensity can be sensitive to an isotope composition of the detector.

The possible existence of a scalar component of gravity waves can also be of potential interest in the light of the NANOGrav data (see Ref. [44]) which allows for the possibility that the observed gravitational-wave signal receives contributions also from monopolar and/or dipolar components. This is impossible in General Relativity, where gravitational waves require a quadrupolar source [90]. However, as discussed above, the confinement mechanism can in principle accommodate additional non-standard contributions into gravitational waves.

PBHs from Real QCD?

In this Section we wish to briefly discuss whether the "real" QCD can be used for realising the presented PBH scenario. At first glance, this looks improbable, since ordinary QCD does not satisfy the necessary condition of all quarks being heavier than the QCD scale Λ_c. Correspondingly, one expects that strings have no chance to last any appreciable time. Even if formed, they will quickly break apart by producing a multiplicity of light quark pairs. However, the situation is more subtle, because for our mechanism the present-epoch values of the quark masses relative to Λ_c are not important. What matters is their values in the early Universe.

As argued in Ref. [91], the quark masses as well as Λ_c can significantly vary during cosmological evolution. The reason is that the expectation values of the fields controlling these parameters change. In fact, in string-theoretic context, where the QCD gauge coupling "constant" is set by fields, such as dilaton and other moduli, the time-variation of Λ_c is a norm rather than an exception. The same is true about the quark masses, since both the Higgs expectation value and Yukawa couplings (which similarly to gauge coupling are determined by moduli) vary.

Therefore, when submerged into a cosmological framework, ordinary QCD can satisfy all requirements of PBH formation scenario by quark confinement. In the present chapter we shall not enter into the details of model building, since our purpose was to point out rather generic aspects of the scenario. However, we wish to remark that its specific realisations can lead to additional potentially interesting correlations with phenomena that are sensitive to Λ_c and m_q. An example is an expansion of the cosmologically acceptable window for the axion field, due to variations of Λ_c and m_q in the early epoch [91].

Due to the electromagnetic charge of QCD quarks, a question may arise whether the electromagnetic backreaction can affect the collapse dynamics. As shown in Ref. [92], the power in photon emission is $P \sim \Lambda_c^4/m_q^2$. This is negligible w.r.t. the initial total energy of the system under condition (3.14) which is assumed throughout this work. Furthermore, as previously mentioned, for the scenario to work with ordinary QCD, the parameter values, such as QCD scale and quark masses must be shifted from their present values. In this case, there is no reason why also the electromagnetic coupling could not have been much weaker during the collapse, therefore suppressing the effect even further.

String-Theoretic Realisation

We wish to briefly discuss a possible string-theoretic realisation of our scenario. We shall not give a full-fledged construction, but merely only point out that string theory contains all the generic key ingredients for it in form of D_p-branes. These represent extended objects, of world-volume dimensionality $p+1$, on which open strings end (for introduction, see Ref. [93]).

It has been known for some time that D-branes can serve as the main engine for driving inflation in string theory [94, 95]. In this scenario, the D-brane tension serves as the source for the energy density required for achieving a temporary de Sitter-like state. In the simplest version, initially, some D-branes and anti-D-branes ($\bar{D}$-branes) are separated by finite distances in compact dimensions, and slowly move towards each other. We note that since D-branes can be wrapped around some of the compact dimensions, the dimensionality of the transverse space in which they are separated can be less than 6. The positive potential energy provided by this configuration (approximately given by the sum of the brane tensions) drives inflation along the 4 non-compact dimensions. The rôle of a slow-rolling inflaton field is played by a brane-separation mode. Upon collision, the D-$\bar{D}$ pairs annihilate, releasing their tension energy into various low-lying string excitations, thereby reheating the Universe.

It was noticed that brane inflation allows production of extended objects much heavier than the inflationary Hubble parameter H_{i}, such as, macroscopic fundamental strings [96]. In the present chapter we shall focus on the production of stringy objects as a result of brane annihilation after inflation. During the process of annihilation of D_p-$\bar{D}_p$, the D_{p-2}-branes are generically produced. The structures that have only two world-volume coordinates in "our" 4 non-compact space-time dimensions, from the point of view of effective 4-dimensional theory, represent D-strings. The characteristic tension of such strings is given by $\mu \sim M_{\mathrm{s}}^2(M_{\mathrm{s}}^n V_n)/g_{\mathrm{s}}$, where M_{s} is the fundamental string scale, g_{s} is the string coupling and n is the the number of compact longitudinal dimensions (wrapped by the D-brane). V_n is the volume of these dimensions. In the simplest case, if the compactification volume is given by the string length, we have $(M_{\mathrm{s}}^n V_n) \sim 1$. Remarkably, as it was argued in Ref. [97], after brane inflation, the production is dominated by above string-like objects. Various aspects of their formation and evolution has been studied in Refs. [98, 99].

We envisage the following implementation of our PBH scenario in this framework. The lower-dimension D-branes, which appear point-like from the 4-dimensional perspective, can be produced as a result of de Sitter fluctuations during the inflationary stage, while the inflation-driving D-$\bar{D}$ system is still functioning. From the point of view of our scenario, such point-like D-defects, play the rôle of "quarks". Their mass can be estimated as $m_{\mathrm{q}} \sim M_{\mathrm{s}}(M_{\mathrm{s}}^n V_n)/g_{\mathrm{s}}$, where n now has to be understood as the number of compact longitudinal dimensions wrapped by a "D-quark", and V_n as the volume of these dimensions. During the stage of brane-inflation, "D-quarks" are inflated away.

Towards the end of inflation, upon annihilation of the "parental" D-$\bar{D}$ system, the string-like D-branes will be produced. We are interested in the case in which they connect the previously produced D-quarks. In such a situation, D-strings play the same rôle as the QCD flux tube played in the confinement case. Our scenario of PBH formation thus should follow.

In this context, it is intriguing to point out a potential connection with gravitational-wave signals observed by NANOGrav (see Ref. [100] for a PBH explanation and Ref. [44] for the original reference). As already discussed in detail in the Sec. 3.3, our scenario would reach the level of this signal for relatively large values of the string tension. These values are reached for a rather conservative choice of string-theoretic parameters. For example, in case of an elementary D_1-string, the parameters are [4]

$$M_{\mathrm{s}} \sim 10^{17-16}\,\mathrm{GeV},\ g_{\mathrm{s}} \sim 10^{-2}\ . \tag{3.28}$$

This appears to be an excellent regime in which the gravitational-wave signal originates from formation of PBHs as dark-matter candidates by our mechanism. For even larger values of the tension, the dissipation in gravitational waves is significant but effective field-theoretic estimates become less reliable.

In the context of a string-theoretic implementation of our mechanism, we would like to comment on the possible presence of non-standard (monopolar and/or dipolar) components as allowed by the NANOGrav data [44]. As already discussed in Sec. 3.3, the presented confinement scenario can potentially accommodate these contributions in the presence of light scalar fields sourced by the endpoints of strings (i.e., heavy quarks or D-“quarks”) and also interacting with the Standard Model particles. Interestingly, in the string-theoretic realisation of our scenario such fields are generic, as there exist scalar moduli that are sourced by the endpoint D-branes. If some of these fields remain sufficiently light or massless, they can be emitted by the D-string/quark systems in modes including the lower multiples.

Of course, as already explained, the same scalar fields are subjected to severe constraints from precision gravitational physics. The reason is that they mediate gravity-competing long-range forces. We cam distinguish two cases.

The first is when the scalar force in question does not violate the equivalence principle (at least, in the sector of the Standard Model particles). This is the case if the scalar is sourced by the trace of the energy momentum tensor $T^{\mu}{}_{\mu}$, which is for instance the situation for the modulus that corresponds to the fluctuations of the entire compactification volume of extra-dimensional space. The phenomenological restriction is that the strength of the force mediated by such a field among ordinary particles must approximately be 10^{-5} times weaker than gravity [101]. The restriction comes mainly from the deflection of star light by the sun.

The second case is when the scalar field in question is not sourced strictly by the trace $T^{\mu}{}_{\mu}$ and has also other couplings. This is for instance the case with the string dilaton.

[4] For effective D_1-strings that are obtained by wrapping the higher extend ($p > 1$) D_p-branes around $p-1$ compact extra dimensions, the same effective tension can be obtained for smaller value of M_{s}.

In this case, the couplings to ordinary matter fields are more severely constrained, since the force mediated by such a field violates the equivalence principle. In case of a dilaton, this violation can be understood from the fact that dilaton sets the values of gauge and gravitational couplings. Due to this, it couples with different strengths to protons and neutrons and correspondingly mediates the isotope-dependent forces among the atoms (see, e.g., Refs. [102, 103]). The phenomenological constraints on such forces bound them to 10^{-12} of gravity [87, 88].

In conclusion, while the string-theoretic version of our scenario contains interesting candidate sources for low-multipole gravitational waves, a non-trivial interplay among the couplings with various sources is required for accommodating the phenomenological constraints from the existing precision gravitational measurements.[5]

Shall the future data be proven to indeed provide the evidence for such gravitational waves, this will boost motivation for finding viable enhancement mechanisms of the mentioned scalar waves.

3.4 Discussion and Outlook

In this chapter we have introduced a novel mechanism for PBH formation, which relies on the production of quarks during the inflationary phase. These are exponentially pushed apart, and get connected by QCD flux tubes after the temperature drops below the confinement scale. Upon horizon re-entry, the quarks accelerate towards each other under the influence of the string tension. The black-hole formation is then triggered by the large amount of energy stored in the string connecting the quark pair.

The presented mechanism does not suffer from exponential fine-tuning, unlike most standard scenarios in which PBHs form from collapse of cosmological overdensities. Moreover, unlike other PBHs which are created during the radiation-dominated epoch and which carry none to very little spin, the confinement mechanism allows for the formation of maximally-rotating black holes, in particular, in the sub-solar mass range as shown in Fig. 3.6. At formation time of a black hole, the impact parameter between the colliding quarks can be as large as the configuration's Schwarzschild radius, therefore leading to maximally-rotating black holes.

In Sec. 3.3 we demonstrated that the PBHs formed by the confinement mechanism can account for the entirety of the dark matter in a mass range around $10^{17} - 10^{19}$ g (see Fig. 3.8). As a by-product, the slowly decaying mass spectrum, scaling as $M_{\rm PBH}^{-1/2}$, could *at the same time* provide seeds for the supermassive black holes observed in the galactic centres. In fact, the right amount of seeds is compatible with 100% of PBH dark matter produced by the same mechanism.

In view of recent arguments that imply a substantial relaxation of the evaporation constraints [see Ref. [80] and Eq. (3.25)], we found that even conservative estimates allow

[5] In the present chapter we shall not enter in a discussion about naturalness of light scalar moduli, as this question is not specific to the present case and is shared by any theory of scalar gravity.

for possible realisations of 100% of the dark matter within our scenario in the mass range 10^4 – 10^{10} g. For masses above the upper end of this range, the standard radiative constraints due to nucleosynthesis, and CMB — although shallower — still applies when using our conservative estimate. However, a complete reevaluation of those constraints, taking the black hole's full quantum structure and dynamics into account, is still missing. This would be of great importance for any scenario in which PBHs of masses below approximately 10^{17} g form. We leave these investigations for future work.

Interestingly, the confinement mechanism of PBH formation could in principle have been driven by ordinary QCD. This is possible, since the time-variation of parameters such as the QCD scale and quark masses are rather generic in inflationary cosmology [91]. Correspondingly, it is not unnatural that the values favourable for the presented mechanism of PBH formation were attained in the early epoch.

We have also outlined a possible implementation of the presented mechanism within a string-theoretic framework of inflation driven by D-branes [94, 95]. In this case, the rôle of heavy "quarks" connected by colour flux tubes is assumed by compact D-branes connected by D-strings. Interestingly, for conservative values of the string-theoretic parameters (3.28), the obtained gravitational-wave signal from PBH formation has the right amplitude in order to be compatible with the events recently detected by NANOGrav, including the possibility to account for possible scalar contributions to the signal.

Chapter 4

Dynamics of confinement

This Chapter mostly overlaps with a work to appear, in collaboration with G. Dvali and S. Valbuena Bermudez [104].

4.1 Introduction

Confinement is the most peculiar property of Yang-Mills theory. A probe pair of quark/anti-quark, if separated by a large distance, will have a linearly growing potential with distance, rather than one which falls off with it. This is a way of understanding why the microscopic degrees of freedom of QCD, quarks and gluons, never manifest themselves alone, but rather they combine into colour-singlets e.g., baryons and mesons. This is always the case asymptotically, namely for distances much longer than the QCD scale d_c.

Such distance has a deep physical meaning. It signals the crossing between two regimes: for energy higher than $\Lambda_c = d_c^{-1}$, quarks and gluons are fundamental degrees of freedom, manifesting themselves asymptotically. Below Λ_c, confinement takes place, and no coloured states are observed.

This scale can easily be computed from the running of the coupling. It corresponds, in fact, to the scale below which the theory stops being perturbative. Above it, the gauge coupling α_c is smaller than one, a phenomenon known as asymptotic freedom. It is inherently due to the presence of gluons, which make the coupling weaker and weaker at higher energies as it can be seen from the one loop running group equation that will be displayed at the end of this Chapter.

Upon reach of Λ_c, the theory becomes strongly coupled and confinement takes place. The theory, in this regime, is still not analytically solved. A natural questions follows: are there physical systems in which the interaction energy between two bodies grows with distance? Is the underlying mechanism well-understood for these system?

This is indeed the case for type II superconductors as predicted by Abrikosov [105, 106]. To understand this, consider two magnets with respectively the north and south pole positioned at the opposite sides of a superconductor. Indeed, within the superconductor the magnetic field lines are not welcomed. However, due to conservation of the $\vec{B}$-lines, a flux tubes forms between the north and the south-poles of the two magnets. Inside it, superconductivity, a consequence of condensation of e.g., a Copper pair, is effectively destroyed. Therefore a linearly growing potential between the two magnets is present, attracting them. This is known as Meissner effect.

Of course, when this phenomenon happens in QCD, the flux tube is non-abelian. Moreover, the confined flux, rather than magnetic, is "coloured". The idea of a dual Meissner effect where "colour" is confined was proposed in [107, 108, 109]. The building blocks of this construction are monopoles. Due to the presence of a condensate breaking the symmetry, and therefore making the "magnetic" photon massive (this is the analogous of the superconductor in the Abrikosov case), these object charge is confined.

The goal of this chapter is to study an explicit realization of this phenomenon, in order to better understand both the underlying mechanism as well as the resulting dynamics. To do so, we focused on the simplest possible field theoretical realization: an $SU(2)$ local theory. This theory explicitly admits monopole, which, upon proper choice of the field content, can be confined.

As a by-product of our analysis, the dynamics of the previous Section, where quarks are confined to form primordial black holes, is also better understood, and explicitly described.

It is found that the point-like limit, which admits an explicit dynamical solution, serves as a good approximation of the full-system, as both the trajectory as well as the resulting gravitational spectrum are well-matched. However, as argued below, the finite-width of the configuration captures novel features, which could be relevant for future astrophysical searches.

Yet another result is the explicit realisation of a sphaleron-like configuration in the confined phase. This corresponds to attaching two strings, the flux tubes confining the magnetic charge of the monopoles, with opposite winding. This can be realised for a monopole/anti-monopole pair with maximal twist. The attachment plane corresponds to a domain-wall dividing the monopole from the anti-monopole. The resulting configuration corresponds to the saddle between two vacua in the gauge sector, and leads to a classically stationary configuration due to the inherent axial symmetry of the system, where the attraction of the confining string is balanced by the repulsive force of the twist. Inevitably, the system is unstable under small perturbations, which leads to the annihilation of the monopoles as expected.

The last part of this chapter is dedicated to the duality between quarks and monopole confinement. In particular, physical arguments are given as to why this classical system properly captures the dynamical annihilation of quarks in the considered parameter space region. This is deeply tied to the saturation of scattering amplitudes discussed in the first two Chapters.

4.1.1 Monopole Confinement

In the previous chapter I described a novel mechanism for producing primordial black holes [39]. Therein, quark pairs, produced and diluted in the inflationary era, are confined in the late Universe and upon horizon re-entry collapse, forming black holes (BHs) due to the large amount of energy stored in the flux tubes connecting them. Given the constant acceleration of quarks sourced by the string, gravitational waves (GWs) of frequency comparable to the inverse of the horizon size are produced.

Previous calculations of the radiated GW power indicate, in the point-like limit, the following emitted power for a large range of frequencies:

$$P_{\mathrm{n}} \sim \frac{\Lambda_{\mathrm{c}}^4}{M_{\mathrm{p}}^2}\frac{1}{n}, \tag{4.1}$$

n being the frequency number, M_{p} the planck mass, and Λ_{c} the confining scale [81]. This relation was derived considering a pair of monopoles connected by a string and is expected to be valid in the fermionic case too. Such sources could explain the recent hints of stochastic GW background obtained from pulsar timing arrays [44, 110]. Moreover, given the flatness of the resulting energy density across several orders of frequency [111], in the future, it will be possible to cross-check, e.g., with LISA.

Motivated by this, the goal of this chapter is to analyze the full dynamics of a monopole/anti-monopole pair in the confined phase in detail. To do so, we consider a $SU(2)$ gauged theory and choose a simple scalar sector capable of achieving the above-mentioned configuration via spontaneous symmetry breaking: a scalar field in the adjoint representation, and a complex scalar doublet. The former breaks the gauge group $SU(2)$ to $U(1)$, therefore admitting t'Hooft-Polyakov monopoles as a solution [112, 113]. The latter breaks the residual $U(1)$ gauge group leading to the confinement of the associated "magnetic flux".

It turns out that the point-like limit approximates very well the fully-fledged classical dynamics of the system. However, we observe annihilation within a time approximately given by the distance, contrary to the point-like case, where an oscillatory behaviour is obtained. Furthermore, the resulting GW spectrum is appropriately captured by the point-like result for scales longer than the monopole width. On the contrary, we observe non-negligible corrections to the power spectrum for scales comparable to the monopole radius, where the emitted radiation is boosted, therefore providing corrections to the GWs emission produced by the confinement dynamics.

A further advantage of this approach lies in the freedom to twist the flux tube connecting the two monopoles [114]. This is done in terms of a twisting angle γ. The maximally twisted case corresponds to the gluing between two strings of opposite winding number. In concomitance to this point, a domain wall form. This configuration in the unconfined case was firstly proposed by [115], and explicitly realized in [114], and has half-integer fermionic charge, analogously to the case of a sphaleron (see e.g., [116]). In this work we analyze such system in the confined case. Due to the metastability of the configuration, the monopole/anti-monopole pair does not annihilate, contrary to the case of non-maximal twist. Instead, it starts emitting soft quanta, and stationarizes at a distance where the repulsive twist force is balanced by the attractive confining force. Eventually, however, instability kicks in, and the monopoles annihilate, dissipating and radiating away the remaining energy.

4.1.2 The role of saturation and relation to quarks

Away from the case of maximal twist, however, the pair always annihilates. A natural question is whether the system, rather than emitting closed incoherent strings, as observed, can, instead, produce a long coherent string connecting a monopole pair – similarly to its initial conditions. Energetically this is possible, since most of the initial energy at the collision moment is in the form of kinetic energy of the monopoles, which are ultra-relativistic.

Namely, as the two monopoles approach each other, the system has no memory of its initial configuration, and effectively, from there onward, the dynamics can be thought of as a

$$few \to many \tag{4.2}$$

scattering process. This is analogous to the systems discussed in Chapter I. In the present case, the asymptotic configuration is played by the long string connecting the monopoles, which is made of coherently organized quanta of soft energy. The production of these many quanta, from only the few ones constituting the initially highly energetic monopoles, is exponentially suppressed.

Contrary to Chapter I, however, a large degeneracy of final states is not present in order to make up for such suppression, and the corresponding scattering amplitude can therefore not be saturated. An immediate way of seeing this is the small symmetry group considered in this example $SU(2)$, i.e., $N_c = 2$. To put it simply, the asymptotic state is undersaturated: it is highly improbable for the two highly energetic monopoles to produce a highly coherent object.

A natural question is how much of the dynamics discussed above applies to the case of confined quarks. Answering this question can shed light on quark confinement: a strongly quantum coupled system can be described in terms of a weakly coupled, classical one.

To address this point, we will focus on the case of heavy quarks, therefore ensuring no breaking of the long string into quark/anti-quark pair. Namely, the lightest quark in the spectrum is much heavier than the confinement scale $m_q \gg \Lambda_c$. In this case, the tunnelling process of the string into quarks pairs is exponentially suppressed. At distances larger than the confinement scale, the quarks "colour" is confined into flux tubes made of gluons. This is analogous to the case of monopoles in the Higgs phase, whose associated "magnetic" charge is confined into a string connecting them.

The resulting dynamics is analogous. The huge energy stored in the connecting fluxes is converted into kinetic energies of the quarks (monopoles) which rapidly accelerate towards each other. Due to the string length being much longer than the confinement scale, these become ultra-relativistic, and can soon be treated as massless. Up to the collapse point, the trajectory is expected to be the same, and effectively depends only on the mass of the quarks (monopoles). What about the moment the string becomes shorter than the confinement length?

At this moment, the energy stored in the quark pair in the form of kinetic energyy is much bigger than the confinement scale. Correspondingly, the gauge coupling evaluated at that scale, as a consequence of asymptotic freedom, is perturbative. This provides further support for the quarks dynamics being captured by the weakly coupled classical dynamics of monopoles. From there onwards, as a consequence of the lack of saturation, also the quark pair is expected to dissipate into incoherent glueballs, rather than producing a classical object.

4.2 Model Setup

We are interested in the dynamics of a long string in the confined phase. The monopole/anti-monopole serves as terminations of the magnetic flux associated to it. We now describe the system allowing for such configuration.

Consider a $SU(2)$ gauged field theory containing a scalar adjoint representation, φ^a, $a = 1, 2, 3$ and a scalar fundamental representation ψ. The system is described by the Lagrangian

$$\mathcal{L} = \frac{1}{2} D_\mu \varphi^a D^\mu \varphi^a + (D_\mu \psi)^\dagger D_\mu \psi - \frac{1}{4} W^a{}_{\mu\nu} W^{a\mu\nu} - V(\varphi, \psi) \tag{4.3}$$

where summation over $SU(2)$ indices is understood, and the gauge field W^a_μ has field strength

$$W^a_{\mu\nu} = \partial_\mu W^a_\mu - \partial_\nu W^a_\mu + g\epsilon^{abc} W^b_\mu W^c_\nu. \tag{4.4}$$

As usual we define the covariant derivatives by

$$D_\mu \varphi^a = \partial_\mu \varphi^a + g\epsilon^{abc} W^b_\mu \varphi^c, \tag{4.5}$$

$$D_\mu \psi = \partial_\mu \psi - ig\frac{\sigma^a}{2} W^a_\mu \psi. \tag{4.6}$$

Finally, the potential is given

$$V(\varphi, \psi) = \frac{\lambda}{4}(\varphi^a \varphi^a - \eta^2)^2 + \frac{\tilde{\lambda}}{2}(\psi^\dagger \psi - v^2)^2 + c\,\psi^\dagger \sigma^a \psi \varphi^a. \tag{4.7}$$

The system in (4.3) has $SO(4) \times SO(3)$ global (softly broken by $c \neq 0$) and $SU(2)$ local symmetry. As it can be seen from the potential (4.7), both fields spontaneously break the symmetry acquiring a vacuum expectation value. Since our main interest is in the case where there is a separation of scales $\eta \gg v$, symmetry breaking happens in two steps.

The adjoint breaks the global symmetry $SO(3)$ to $SO(2)$. The associated vacuum manifold is a two-sphere $\mathcal{S}_2$. Correspondingly the second homotopy group is non-trivial

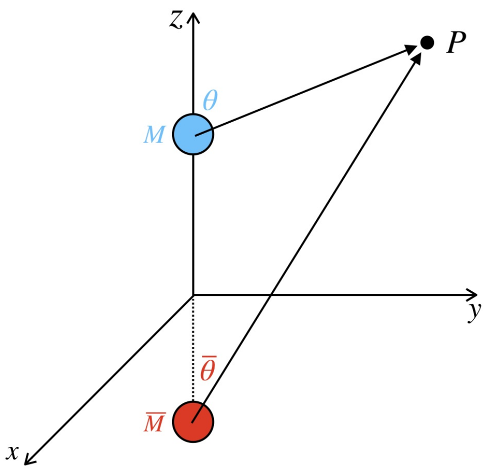

Figure 4.1: A sketch of the initial monopole/anti-monopole initial configuration.

and monopoles configurations are admitted. From the local side of things, the symmetry is broken down to $U(1)$ and two gauge fields become massive. We refer to this phase as Coulomb.

Upon spontaneous symmetry breaking of ψ, for $c \sim 0$, the global symmetry $SO(4)$ is broken down to $SO(3)$. This is similar to Higgs doublet global symmetry in the Standard Model whose global residual symmetry is $SU(2)_{custodial}$. For non-vanishing c coupling the actually symmetry is $SO(2) \times SO(2)$, which is broken to $SO(2)$. The previously massless gauge boson, now becomes massive, therefore confining the associated "magnetic" flux of monopole into strings. This is referred to as the Higgs phase. The dynamics of monopoles during the latter phase transition is the main focus of this Chapter.

4.3 String realization

In Fig. 4.1 a sketch of the initial configuration studied in this work is shown. A monopole and anti-monopole are positioned along the z-axes, and have, initially, a distance d. For simplicity we denote with θ and $\overline{\theta}$ the azimuthal angle of the monopole and anti-monopole respectively. In the Coulomb phase, this can be though as a magnetic dipole configuration. The string connecting them, can easily be guessed, providing us with ψ. For $\overline{\theta} = 0$, a monopole should be recovered $\psi \propto (\cos\theta/2, \sin\theta/2e^{i\phi})^t$, while for $\theta = \pi$ an antimonopole should be obteined $\psi \propto (\sin\overline{\theta}/2, \cos\overline{\theta}/2e^{i\phi})^t$, ϕ being the polar angle. Therefore the string configuration is given by [117, 118, 114]

$$\psi \propto \begin{pmatrix} \sin(\theta/2)\sin(\bar{\theta}/2)e^{i\gamma} + \cos(\theta/2)\cos(\bar{\theta}/2) \\ \sin(\theta/2)\cos(\bar{\theta}/2)e^{i\phi} - \cos(\theta/2)\sin(\bar{\theta}/2)e^{i(\phi-\gamma)} \end{pmatrix}. \tag{4.8}$$

Above γ is responsible for the twist between monopole and anti-monopole. This can be seen from the fact that for $\theta = \pi$, ψ indeed describes an anti-monopole similarly to the one above. However, the polar angle needs to be shifted $\phi \to \phi + \gamma$. In the upper hemisphere we have, for $\theta = \overline{\theta} = 0$, $\psi = (v, 0)^t$, while in the lower hemisphere, for $\theta = \overline{\theta} = \pi$, $\psi = (ve^{i\gamma}, 0)^t$. In between, connecting the two monopole, we have a unit winding string, i.e., for $\theta = \pi$ and $\overline{\theta} = 0$, $\psi \propto (e^{i\phi}, 0)^t$.

Far from the monopoles, the string (4.8), is proportional to the third Pauli matrix positive eigenvector. Given that in our study, the last interaction term in (4.7) was chosen negative $c < 0$, the adjoint field unit vector $\hat{\varphi}^a$ for the monopoles is asymptotically given by [117]

$$\hat{\varphi}^a = \frac{1}{v^2}\psi^\dagger \tau^a \psi, \quad a = 1, 2, 3 \tag{4.9}$$

where τ^a are the three Pauli matrices (see Fig. 4.3 below).

In the next Section we analyze the monopole/anti-monopole configuration after the first phase transition, ignoring the doublet. Although this was already done in [118, 114] it serves as a useful exercise before turning to the symmetry broken phase.

4.4 Monopole/anti-monopole system

The explicit equations of motion can be found in Appendix B. For simplicity, from now on, the gauge coupling $g = 1$ and all dimensionfull quantities are expressed in terms of η which is also set to unity. Before proceeding we note that λ is the parameter of the theory determining the mass and size of the monopoles.

The field configuration of a single monopole is given by [112, 113]

$$\varphi^a = h(r)\hat{r}^a, \quad W_i^a = \frac{(1 - k(r))}{r}\epsilon^{aij}\hat{r}^j, \tag{4.10}$$

where r is the radial coordinate and its norm is given by $\hat{r}^a = r^a/|\vec{r}|$. Under ansatz (4.10), a stationary configuration can be found by solving the following equations of motion

$$h''(r) + \frac{2}{r}h'(r) = \frac{2}{r^2}k(r)^2 h(r) - \lambda(h(r)^2 - 1)h(r), \tag{4.11}$$

$$k''(r) = \frac{1}{r^2}(k(r)^2 - 1)k(r) + h(r)^2 k(r), \tag{4.12}$$

supplemented with the following asymptotic conditions

$$h(r) \xrightarrow{r\to 0} 0, \;\; k(r) \xrightarrow{r\to 0} 1, \tag{4.13}$$

$$h(r) \xrightarrow{r\to\infty} 1, \;\; k(r) \xrightarrow{r\to\infty} 0. \tag{4.14}$$

The above equations can be solved numerically. The resulting profile is shown in Fig. 4.2.

We are now ready to generalize the ansatz (4.10) to the case of interest of a monopole/anti-monopole as

$$\varphi^a = h(r_m)h(\bar{r}_m)\hat{\varphi}^a, \tag{4.15}$$

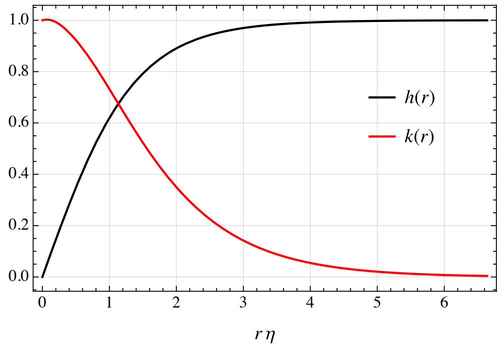

Figure 4.2: Monopole profile.

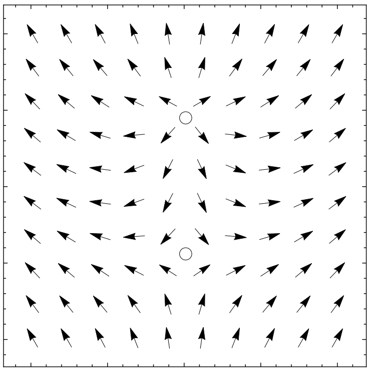

Figure 4.3: Example of field configuration $\hat{\varphi}^a$ for twist $\gamma = 0$ according to Eq. (4.15) in the yz plane. The circles denote the monopoles position.

with r_m ($\bar{r}_m$) being the radial distance from the monopole (anti-monopole) center and $\hat{\varphi}^a$ is defined in (4.9). An example of such configuration is shown in Fig. 4.3.

The gauge field ansatz follows from the usual requirement of vanishing covariant derivative of the Higgs isovector at spatial infinity, $D_\mu \hat{\varphi}|_{r\to\infty} = 0$, giving

$$W^a_\mu = -(1 - k(r_m))(1 - k(\bar{r}_m))\epsilon^{abc}\hat{\varphi}^b \partial_\mu \hat{\varphi}^c. \tag{4.16}$$

As expected, the monopole/anti-monopole attract each other in a Coulomb-way due to their magnetic charge. We verified this behaviour, which was firstly analysed numerically for this system in [114]. It was also shown there, that the potential energy of the system depends on the twist γ as firstly suggested by [115].

Verifying these properties served as a valuable check of the numerics presented in this work.

4.5 Monopole/Anti-monopole connected by strings

Eqs. (B.1,B.4) were solved numerically, with initial conditions given by the monopole/anti-monopole ansatz (4.15) and (4.16). Before the evolution, the system was numerically relaxed, with a similar method as the one used in [114].

Far from the monopoles, $\varphi^a = \eta\delta^{a3}$, implying that ψ, due to the last interaction term in (4.7), needs to be proportional to the positive σ^3 eigenvector $\langle|\psi|\rangle \propto (1,0)^t$, as correctly described by ansatz (4.8)[1].

ψ minimizes the interaction energy above the pair. Crossing the monopole, the configuration becomes singular. Namely, at the monopole south pole the phase changes by 2π. As a consequence, between the monopoles, along the z-axis, $\psi \propto (0, e^{i\phi})^t$, where ϕ is the polar angle. The associated winding number is, by construction, unity. At the north pole of the anti-monopole, the string flips again by 2π and is, thereafter proportional to $\psi \propto (e^{i\gamma}, 0)^t$.

The potential energy is independent from the explicit value of γ. However, the same is not true for the kinetic terms of both scalar and gauge fields. In fact, $\gamma \neq 0$ leads to an extra repulsive interaction [114] between the pair, which is maximal for $\gamma = \pi$. The consequences of such interaction will be described later, and, for now, we focus on the case $\gamma = 0$.

As the "magnetic" field of the pair confines into tubes, the monopole/anti-monopole pair accelerate towards each other, turning relativistically, and, finally, annihilates. In

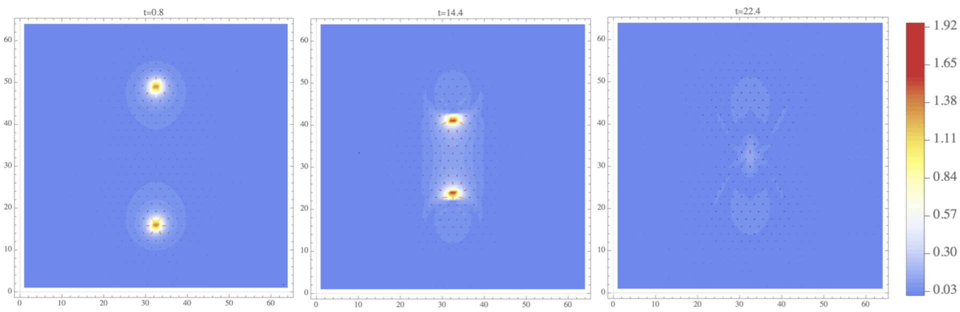

Figure 4.4: Magnetic Field Evolution.The colour bar corresponds to the magnitude.

Fig. 4.4, snapshots of the time evolution of the "magnetic" field are shown. The string forms at early times.

The magnetic field is neutralized by the longitudinal massive photon component i.e., the eaten Goldstone boson [35]. Effectively, the system behaves as the type II superconductor described in the Introduction. Moreover, due to compactness of the $SU(2)$ group, no residual magnetic charge is observed. In fact, the confining string, related to the breaking of the $U(1)$ subgroup, has same charge units as the monopoles, ensuring a complete neutrlization of the magnetic field. Regarding this point, it should be noted that numerically this was verified for big enough volumes. If the lattice size was too small, some of the monopole charge would be "trapped" at the boundary, resulting in some net magnetic field at the end of the simulation. This, of course, was just an artefact of numerics.

[1] we chose $c \leq 0$ in our numerical simulations

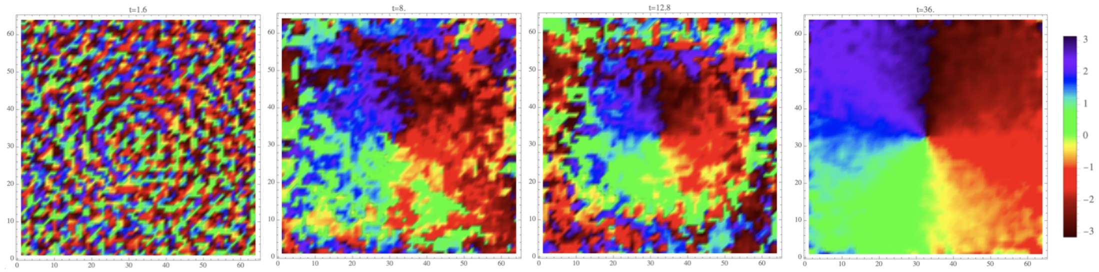

Figure 4.5: Phase of the confining scalar field in the xy plane at the middle of the string height.

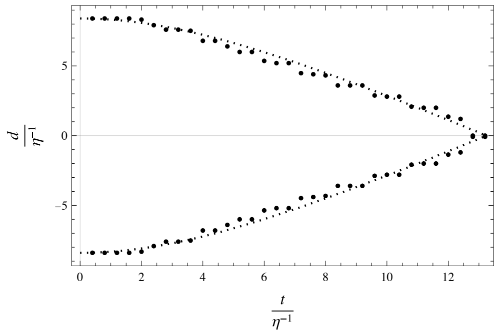

Figure 4.6: Time evolution of the position of the cores of the monopole and anti-monopole. The dots are numerical results while the dashed line is the point-like solution (4.18). Here $a = \mu/m_m = 0.16\eta$.

An explicit example of string formation is shown in Fig. 4.5. The figure shows the phase of the field ψ along the xy plane, in between the two monopoles. Therein, the initial phase of ψ was randomized at each lattice point. As it can be seen, a clear string structure with winding one emerges. Motivated by this, from now on, we use the initial conditions mentioned at the beginning of the Section.

The dynamics shown in Fig. 4.4 is appropriately approximated by the point-like solution found in [81] as we are about to show. The action of the system considered by Ref. [81] is

$$I = -m_m \int ds_1 - m_m \int ds_2 - \Lambda_c^2 \int dS, \tag{4.17}$$

in which the monopole/anti-monopole worldlines are determined by the first two terms, while the last one addresses the string world-sheet. Extremization of (4.17) leads to the equations of motion for the system, which admits a particular solution consisting of a monopole pair connected by a straight string. The resulting monopoles trajectories are found to be [81]

$$x(t) = \pm \frac{\mathrm{sgn}(t)}{a}(\gamma_0 - \sqrt{1 + (\gamma_0 v_0 - a|t|)^2}) \tag{4.18}$$

where $t_0 = -\gamma_0 v_0/a$, $a = \Lambda_c^2/m_m$, v_0 and $\gamma_0 = (1 - v_0^2)^{-1/2}$ are respectively the maximum

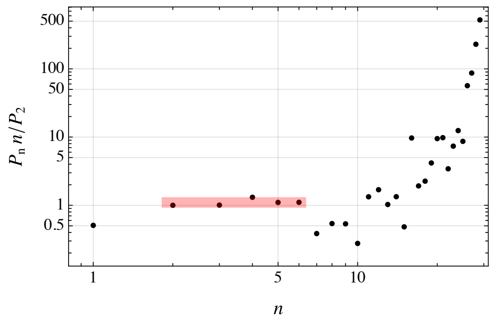

Figure 4.7: Angularly integrated power emitted P_{n} according to (4.20). The amplitude was normalized w.r.t. to the lowest frequency comparable to the initial monopoles distance. Up to frequencies comparable to the monopoles size $P_{\mathrm{n}} \propto n^{-1}$ (shaded region).

velocity and Lorentz factor of the monopoles, reached at $t = 0$. This describes a pair of relativistic monopoles, connected by a string, oscillating around their center.

The resulting dynamics is shown in Fig. 4.6 where it is compared with the actual numerical result. The black dots stands for the numerical position of the monopoles center in the fully-fledged field theoretical study. As it can be seen, they are nicely fitted by solution (4.18) (dashed line). Indeed, as anticipated, the monopoles, under a constant acceleration, become relativistic. However, in our study, upon approaching each other, they annihilate, contrary to what is seen in the point-like case, where they, instead, miss each other, and undergo an oscillatory motion around the starting center of the configuration.

4.5.1 Gravitational Waves

We wish now to evaluate the resulting gravitational wave spectrum of our dynamics, and to compare it to the point-like study of Ref. [81]. The radiated gravitational power at frequency $\omega_n = 2\pi n/T$ (T being the collapse time)[2], per unit solid angle in the direction $\mathbf{k}$, $|\mathbf{k}| = \omega_n$ is given by [119]

$$P = \sum_n P_n = \sum_n \int d\Omega \frac{dP_n}{d\Omega}, \tag{4.19}$$

$$\frac{dP_n}{d\Omega} = \frac{G\,\omega_n^2}{\pi} \left(T^*_{\mu\nu}(\omega_n, \mathbf{k}) T^{\mu\nu}(\omega_n, \mathbf{k}) - \frac{1}{2} |T^\mu_\mu(\omega_n, \mathbf{k})|^2 \right). \tag{4.20}$$

Above the energy-momentum tensor in Fourier space is defined as

$$T^{\mu\nu}(\omega_n, \mathbf{k}) = \frac{1}{T} \int_0^T dt\, e^{i\omega_n t} \int d^3\mathbf{x} e^{-i\mathbf{k}\cdot\mathbf{x}} T^{\mu\nu}(t, \mathbf{x}). \tag{4.21}$$

In Fig. 4.7, the radiated gravitational spectrum $P_n\, n$ as a function of n over logarithmic intervals due to the collapse is shown. As it can be seen, for low frequencies, $n \lesssim 7$ (red

[2]For practical purposes we chose $T = 2d\eta^{-1}$, d being the lattice distance between monopoles.

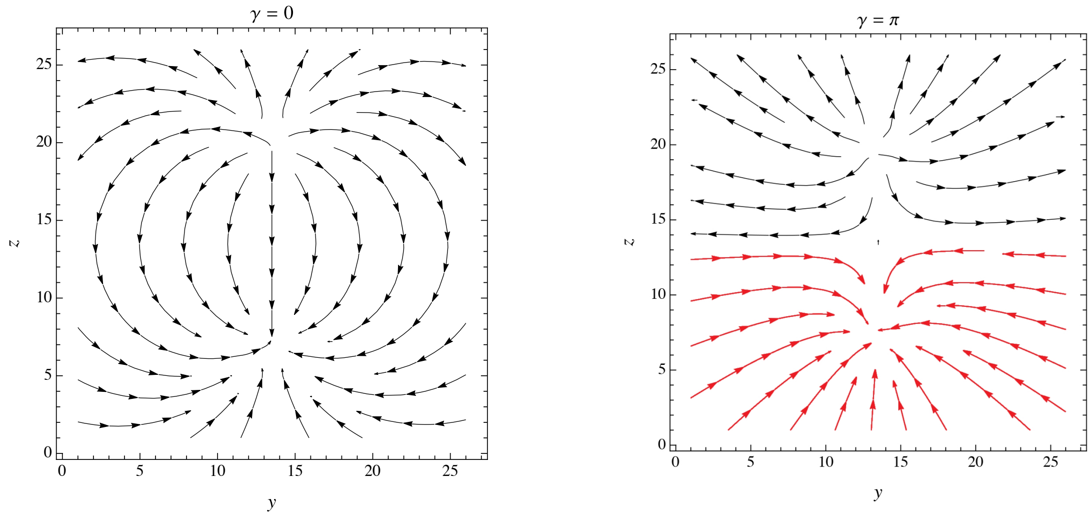

(a) (b)

Figure 4.8: Initial magnetic field configuration comparison for $\gamma = 0, \pi$.

shaded area in the plot), the spectrum is $P_n \sim n$ which is the same scaling found in the point-like study [81]. This is easy to understand: such wavenumbers corresponds to lengths longer than the string and monopoles width, and therefore the system can be considered effectively point-like.

Differently from the point-like result, however, near annihilation the radiation spectrum is boosted, for frequencies comparable to the width of the system. No exact scaling was found in this region of frequencies. However, suffices to say that this is very different from the point-like case where the spectrum is expected to decay even faster. Higher modes have are not displayed in 4.7, as their inverse becomes comparable to the lattice spacing, and therefore could be unreliable.

4.5.2 Twisted case

So far we have been focused on the untwisted configuration i.e., $\gamma = 0$. This corresponds to an energetic minimum of the string energy. While it is obvious from (4.8) that rotating γ by 2π gives back the same configuration, it is straightforward to see how the energy varies with γ (at fixed distance d) and find that $\gamma = \pi$ is an energy maximum.

In Fig. 4.8, the effect of the twist on the initial magnetic field configuration is shown. While for the case $\gamma = 0$ (a) the magnetic field lines connect between monopole and anti-monopole, in the twisted case $\gamma = \pi$ (b) the situation is dramatically different. The magnetic fields do not close on the monopoles and open up. This configuration corresponds to gluing two string with opposite winding number. At the gluing plane, $z = z_*$, the string phase becomes singular, and inverts itself, resulting in the magnetic field shown in the Figure. This effectively results in a domain wall between the upper and lower part of the

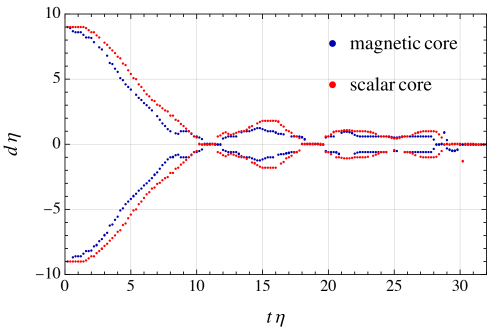

Figure 4.9: Evolution of the magnetic and scalar cores of the monopole/anti-monopole pair for initial twist $\gamma = \pi$.

system as shown in Fig. 4.8. The symmetry of the configuration, $\gamma = \pi$, provides a further rationale for this to be an energy maximum.

While perturbations are indeed expected to break the enhanced symmetry of the configuration, allowing the system to relax to the energy minimum of the zero-charge sector, it is clear that independently of the phase of the system – Coulomb or Higgs – there will be a repulsive force between the two monopoles, forbidding their annihilation at the classical level. Refs. [114, 120] numerically verified the behaviour of this object in the unconfined case, and observed how for twist $\gamma = \pi$ the monopole/anti-monopole, attractively interacting via the Coulomb potential, do not annihilate due to the repulsive effect of the twist. To our knowledge, the behaviour of this configuration in the confined phase has not been addressed so far.

The dynamics in the confined phase is shown in Fig. 4.9 where the position of the two monopoles core centers is shown as a function of time. As it can be seen, at initial time the two magnetic cores start to accelerate towards each other due to the flux tubes connecting them, dragging the scalar core along and the system turns relativistic.

The dynamics is analogous to the untwisted one, c.f. Fig. 4.6, up to the collapse moment. While in the untwisted case the two monopoles simply annihilates, in this case the magnetic cores repel each other and slow down, as they cannot annihilate due to the relative twist. While for $\gamma \neq \pi$ this was verified never to happen, as the two monopoles can easily untwist in the direction of the more favourable minimum, for $\gamma = \pi$ the string cannot unwind, and a metastable configuration is obtained.

From there on the two monopoles have a bouncing behaviour, and dissipate energy up to settling to a constant distance where the confining energy is balanced by the repulsive twist energy. Eventually the metastable configuration becomes unstable and the pair fully annihilates. Concomitantly a deviation from axial symmetry is observed. Given the axial symmetry of the initial configuration, and the fact that the dynamics should preserve such symmetry, we believe this to be a numerical artefact.

In Fig. 4.9 $\Lambda_c = \eta$ was used. For lower value of this parameter the bouncing sizes, as well as distance of the bound state were observed to be larger.

Relation to sphaleron

Ref. [116] found a sphaleron solution in the electroweak theory with baryonic charge 1/2. We show here, that for $\gamma = \pi$, configuration (4.8), describing a fully twisted monopole/anti-monopole pair gives the same result. This offers an interpretation of the solution found by [116] as suggested by Ref. [121]. We focus here only on the $SU(2)$ group for simplicity.

A massless $SU(2)$ charged chiral fermion χ has a current

$$j^{\mu} = \overline{\chi}\gamma^{\mu}\chi, \tag{4.22}$$

whose divergence receive the anomalous contribution

$$\partial_{\mu} j^{\mu} = \frac{g^2}{64\pi^2}\epsilon^{\mu\nu\rho\sigma} W^a_{\mu\nu} W^a_{\rho\sigma}. \tag{4.23}$$

It follows from (4.23), that if the gauge and Higgs fields are time dependent, so is the chiral fermionic charge. In particular, if the fields interpolates between two vacua via an incontractible loop, then the femionic charge is expected to change by an integer. By symmetry reasoning, the sphaleron, namely the configuration at the top of the barrier between these two vacua, is expected to have fermionic charge 1/2.

Assuming the baryonic flux of the three volume to vanish, the change of fermionic charge can be obtained (noticing that the right hand side of (4.23) is the total derivative of the Chern-Simon form). This leads to the Chern-Simon number

$$Q(sphaleron) = \frac{g^2}{32\pi^2}\int d^3x \epsilon_{ijk}\left(W^{aij}W^{ak} - \frac{g}{3}\epsilon_{abc}W^{ai}W^{bj}W^{ck}\right). \tag{4.24}$$

Eq. (4.24), must be evaluated in the right gauge, namely, it must be ensured that at spatial infinity the spatial part of the Chern-Simon form decays faster than $1/r$. This can be done via the gauge transformation [116]

$$U(\vec{x}) = \exp\left[\frac{i}{2}\Theta(r)\vec{\sigma}\cdot\vec{x}\right], \tag{4.25}$$

where $\Theta(r)$ is an arbitrary function chosen to approach π sufficiently fast as $r \to \infty$. By plugging (4.16) under gauge transformation (4.25) in (4.24), it is straightforward to see

$$Q(sphaleron) = 1/2 \tag{4.26}$$

as expected. The result of this analysis, performed in the Coulomb case, was verified to numerically hold also in the confined case.

4.6 Heavy Quark Annihilation

This section is dedicated to showing the existence of a remarkable correspondence between the scattering of monopoles and the scattering of heavy quarks in QCD. For simplicity, consider a heavy quark in the fundamental representation of a gauged $SU(N_c)$. By "heavy" here, it is meant that the quark mass m_q is much higher than the QCD scale, Λ_c. No light quarks are assumed to exist in the theory and the quark spin is unimportant fore the analysis that follows.

The four-point gluon function, is determined by the fundamental coupling α_c. For later convenience, we also define the 't Hooft coupling $\lambda_t \equiv \alpha_c N_c$ [15] and work in the large N_c limit.

In this theory the scale Λ_c has an important physical meaning, namely, it divides two descriptions. For distances smaller than the QCD length $L_c \equiv \Lambda_c^{-1}$, the theory is described in terms of weakly interacting gluons and quarks. At lower energies, namely for distances bigger than L_c, confinement takes place, and fundamental degrees of freedom become colourless composites e.g., glueballs and mesons.

In this phase, when sources are separated by a distance $d \gg L_c$, the gluon "electric" field is trapped in a flux tube connecting the two. This is the essence of the description, which can be thought as a dual version of Meissner effect.

In the previous Sections the dynamics of monopoles with confined "magnetic" charge is addressed. A pair of quark/anti-quark connected by a QCD string is strikingly similar to such system. The monopole (anti-monopole) is mapped on quark (anti-quark). Magnetic flux tube is mapped on the QCD string.

A natural question is how much of QCD physics is captured by the above correspondence. The $SU(2)$ monopoles are confined as the theory enters the Higgs phase. Correspondingly, the resulting solitonic object is made of fundamental degrees of freedom (scalar and gauge bosons) in the weak-coupling regime. Therefore, the system is well-approximated by the classical dynamics.

In the dual QCD case, constituents are confined and strongly coupled, a fact that makes such correspondence rather difficult to establish. Any hint bypassing this problem, is a fundamental step-forward in our understanding of QCD physics: a strongly-coupled quantum system, the one of confined quarks pairs, could be described in terms of a weakly-coupled classical one, i.e., monopoles connected by "magnetic" flux tubes.

Now, we would like to show evidence that the above numerical simulation captures the dynamical behaviour of confined quarks pairs in the following sense. Namely, we observe that in the head-on scattering of this system, a long-classical string is never recreated. The pair always annihilate and radiates aways. We provide arguments as to why the same behaviour is expected for quarks when considered in the same kinetic regime.

Before proceeding it is worth mentioning that here we will not be dealing with the twisted case discussed in the previous Section. In that case, for $\gamma = \pi$, a meta-stable configuration is obtained. In fact, the monopoles do not annihilate immediately, but rather radiated quanta, and stabilize at a distance where the repulsive twist interaction is balanced by the string energy connecting them. Because most of the initial energy of the system has been radiated away, upon relaxation to the zero-charge vacuum (when the two monopoles annihilate), there is not enough energy to recreate a long-classical object as the initial one.

Surprisingly, even for $\gamma = 0$, when the monopoles annihilate right away, even though the system has enough energy to produce a long classical string, this never happens. Notice that in our analysis, the initial energy of the configuration is much bigger than the monopoles mass $d\mu \gg m_m$ which is clearly subdominant. This leads to a relativistic acceleration of the string ends. When the quarks are about to annihilate, at a distance comparable to the string width $L_c \equiv \Lambda_c^{-1}$, their kinetic energy is of order $\sim d\Lambda_c^2 \gg m_m$, and can therefore be treated as massless.

The same analysis applies when describing the dynamics of confined quarks, under the replacement $m_m \to m_q$. It should be mentioned that the following hierarchy of scales is necessary

$$\Lambda_c \ll m_q \ll d\Lambda_c^2, \tag{4.27}$$

where the first inequality ensures the stability of the string under nucleation of quark pairs, and the last one ensures that the quark/anti-quark pair is relativistic as they approach each others.

The key-point is that the quarks scattering length, when they are at a distance Λ_c^{-1}, is much shorter than the QCD confining scale $L_c \sim \Lambda_c^{-1}$, i.e.,

$$r_* \sim \frac{\alpha_c}{d\Lambda_c^2} \ll \Lambda_c^{-1}, \tag{4.28}$$

where α_c is the QCD running coupling evaluated at energies r_*^{-1}; this is much higher than the confinement scale, Λ_c, and therefore α_c is weak, as it can be understood from the 1-loop renormalization group flow of the QCD gauge coupling

$$\alpha_c(r_*^{-1}) = \frac{2\pi}{b \log\left(\frac{r_*^{-1}}{\Lambda_c}\right)}, \tag{4.29}$$

where $b = \frac{11}{3}N_c - \frac{1}{3}N_f$, N_c being the number of colours and N_f the number of flavours of quarks in the theory (assumed to be in the fundamental representation for simplicity).

Thus, the quark-anti-quark scattering can be evaluated in the weak coupling regime. However, we must keep in mind that the multiplicity N_c of the produced quanta is large and the collective effects, controlled by a product $\alpha_c N_c$, must be taken into account.

The products of the scattering, at distances of order Λ_c^{-1} hadronizes, forming colourless states. A natural question is whether this can consist of a long stretched string, or to many closed strings (glueballs) and open strings (mesons). This is due to the exponential suppression of the former process when considering a

$$2 \to n \tag{4.30}$$

transition, as discussed in [4] and summarized in Chapter I.

The question is whether the summation over final degenerate micro-states can make up for such exponential suppression: this can happen if the classical configuraiton is at saturation. As we will argue below, this is not the case for the considered system.

Entropy of the string

The number of microstate of a straight QCD string of length d is given by all possible distinct orientations

$$n_{st} \sim \frac{d^2}{L_c^2}, \tag{4.31}$$

leading to a string entropy much smaller than the maximal saturation entropy

$$S_{string} \sim \log\left(\frac{d^2}{L_c^2}\right) \ll S_{sat} \sim \frac{d^2}{L_c^2}, \tag{4.32}$$

for the case $d \gg L_c$ considered in the numerical simulations.

This shows that the string entropy is not sufficient to make up for the exponential suppression due to the (4.30) process which we are about to estimate explicitly.

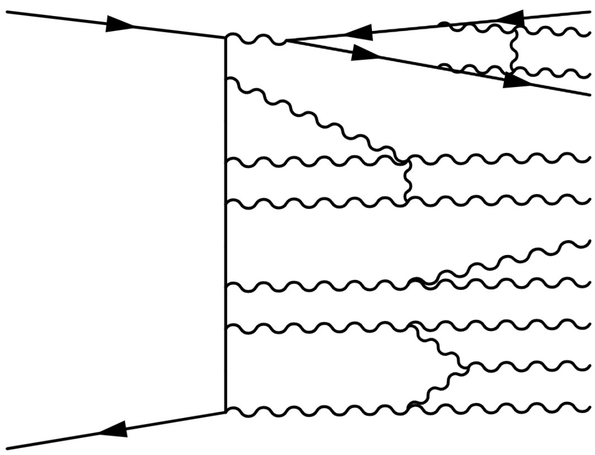

Figure 4.10: Quark pair annihilates into gluons, which produce a quark pair and gluons.

Before that, let us note that different types of diagrams can contribute to (4.30). In the first case, the quarks can annihilate into gluons which then produce the quark pair plus other gluons as shown in Fig. 4.10. Another possibility, is that quarks scatters without annihilating, producing several gluons (see Fig. 4.11 for an example). Yet another possibility is a system producing several short open strings, namely mesons as in Fig, 4.12.

The first two cases both consist of a quark-pair accompanied by several soft-gluons as outgoing states. These can be organized in the form of a classical long string, or in form of short closed strings (namely glueballs) [3].

The point is that due to the lack of saturation of entropy (4.32), the former is exponentially suppressed with respect to the latter. Equally stated, it is more probable for the system to produce many incoherent glueballs rather than a coherent classical long string

[3]These are fundamental deggrees of freedom in the confined phase, and therefore the resulting state is quantum.

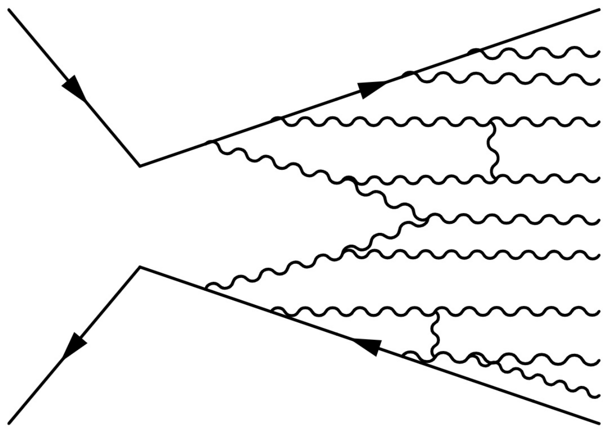

Figure 4.11: Quarks scattering into gluons without annihilation.

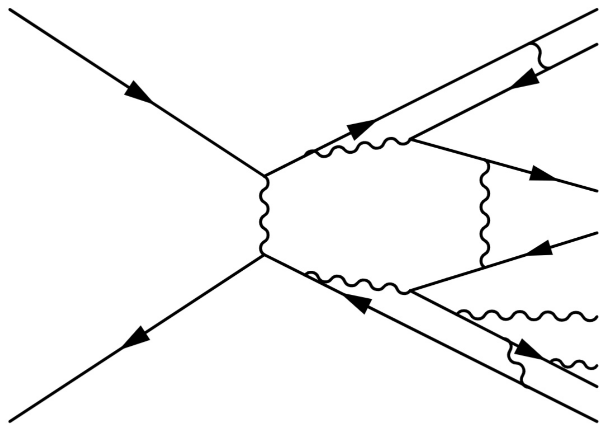

Figure 4.12: Quarks annihilation into mesons.

made of highly coherent gluons. Simply put, the first case has a much higher entropy than the other.

Gluon picture: Understanding suppression from the entropy of multi-gluon state

A long classical string can be thought of as a state with a high-occupation number n of gluons. For illustrative purposes and clarity we work in the 't Hooft limit, $N_c \to \infty$, $\lambda_t =$ finite.

Our focus is the scattering of two hard quanta, into n soft gluon. The resulting final state is a colour singlet, however, its microstate entropy is enhanced due to the colour group representation being big. This enhances the transition probability as shown in [4].

In this limit the fundamental coupling is weak but collective coupling is finite. In this theory we are interested in production of a state of high occupation number n of soft gluons out of the initial high energy state of few hard quanta. The gluons are soft quanta of De-Broglie wavelength $\sim d$, and therefore their number can be estimated to be $n \sim d^2\Lambda_c^2$. Ignoring, for a moment, the contribution due to the degeneracy of microstates, this leads to the following suppression, analogous to the one found in Chapter I

$$\sigma_{2\to N} \simeq e^{-n} \tag{4.33}$$

The n-gluon state forms a large representation of the colour group and effectively has a high microstate entropy. This enhances the transition probability. Of course, the string is colourless, but this simply means that the final physical state is averaged over colour.

Simple microstates counting leads, for $\lambda_t \sim 1$, to the same result found in Chapter I [4], that is

$$\sigma = \sum_{microstates} \sigma_{2\to n} \simeq e^{-n} \left(\frac{en}{N_c}\right)^{N_c}. \tag{4.34}$$

Namely, saturation of unitarity takes place only for $N_c \sim n$. In our numerical analysis, however, $N_c \sim 1$, while $n \gg 1$ from which follows

$$\sigma \sim e^{-(d\Lambda_c)^2}. \tag{4.35}$$

This shows the exponential suppression of the process.

Basically, in the language of [4], the long string is an strongly undersaturated object. Correspondingly, the cross section for its production is exponentially suppressed. This is the underlying physical reason for non-observation of the re-production of a long string in a head-on collision of confined monopoles. The same picture holds for confined quarks.

Indeed there exist others regimes where the string is unsuppressed. For example, this is the case when the energy of quarks is less than $4m_q$ but still much larger than Λ_c. In this case the string of length $L = 2m_q/\Lambda_c^2$ can be created.

For initial energies much bigger than $4m_q$, it is natural to ask whether increasing the number of quark flavours can make up for the lack of saturation. This is not possible as it can be seen form Eq. (4.29) and below. In fact, if the number of flavours increases too much, the asymptotic freedom of the theory is spoiled.

4.7 Outlook

In this chapter we numerically studied the confinement of a $SU(2)$ monopole/anti-monopole pair. Initially the pair is in a dipolar configuration as in Fig. 4.3. The confinement is instantaneously imposed by setting an extra complex doublet field in its Higgs-phase, therefore breaking the residual $U(1)$ and giving mass to the previously massless "photon". In this sense the considered initial configuration is similar to a first order phase transition, where the pair is suddenly in the confining phase.

As shown in Fig. 4.6, the monopoles become immediately relativistic due to the confinement of the magnetic flux inside the cosmic string connecting them. Taking initial random phases for the confining scalar field, it is possible to see the dynamical emergence of the tube as shown in Fig. 4.5.

The GW spectrum is also computed and is well-approximated by the point-like study of Ref. [81] for wavelengths longer than the relevant widths of the system (i.e., monopoles and string width). Namely, we confirm a power spectrum $P_n \propto n^{-1}$, n denoting the frequency number. As previously mentioned, this type of spectrum can lead to a flat density of GWs Ω_{GW} across several orders of the frequency, therefore making it interesting from a phenomenological perspective in view of future refinement of the stochastic GW background hints obtained from pulsar timing arrays [44, 110]. Due to the low frequency range of the detection – inverse years – a natural mechanism for the production of the necessary initial configuration i.e., of a long cosmic string connecting the pair is proposed in Ref. [39], where the cosmic string is exponentially long due to the inflationary dilution of the later confined quarks.

Differently from the point-like study, we observe that for initial configurations of energies much higher than the monopole mass, the head-on collision always results in the annihilation of the monopole, and the energy of the configuration dissipates away. This is always the case unless the twist is maximal i.e., $\gamma = \pi$. This case corresponds to the gluing of a string with a string of opposite winding number. Effectively, a domain wall is present at the junction point as shown in Fig. 4.8b. The resulting configuration, upon confinement, is a metastable one: the repulsive energy of the twist is balanced by the attractive string tension as shown in Fig. 4.9. This configuration is the generalization to the confined case of the solution found in [116]. Its meaning in terms of vacuum structure is clear: it corresponds to the lowest maximum along the path interpolating between two $SU(2)$ gauge vacua i.e., a sphaleron. To support this, its fermionic charge is shown to be half-integer. Indeed, being a maximum, as the instability kicks in, the configuration relaxes to the $Q = 0$ vacuum, the strings untwist, and the monopole annihilates, dissipating the remaining energy.

For $\gamma \neq \pi$, the monopoles always annihilates immediately. In particular, it is argued why the same behaviour is expected for the case of a confined quark/anti-quark pair in the same kinematic regime. In particular, it is shown that the reason why the system annihilates, rather than forming another long string, analogous to the initial condition, is tied to a lack of entropy saturation of such classical objects. in fact, a $2 \to n$ process is generally exponentially suppressed. In Chapter I, we showed how a large microstate degeneracy of final states can make up for the suppression, leading to the formation of a highly coherent classical object, made of soft-quanta of De-Broglie wavelength d. A necessary condition for this to happen is $n \sim N_c$, or equivalently, that both collective couplings $\lambda_c = \alpha_c n$ and $\lambda_t = \alpha_c N_c$ are of order unity and therefore saturate scattering unitarity. Correspondingly, such configurations have a maximally entropy equal to their area measured in units of Goldstone decay constants associated to the symmetries broken by the the configuration itself.

In the system considered numerically, $N_c \sim 1$, and therefore saturation is not possible. Therefore, the process of formation of a very long classical string is exponentially suppressed with respect, e.g., to the process where small closed-string loops are produced in an incoherent way. The same argument applies to the case of quarks.

The end result is striking: in this kinematic regime, the dynamics of two highly relativistic quarks colliding head on – a very quantum state –, is captured by the classical evolution of two collapsing monopoles in the weak-coupling regime.

Appendix A

Newton Raphson method

In this Appendix we describe the algorithm used to obtain the profile of the vortex in the non-topological soliton.

In two dimension the vortex profile has only radial dependence, and therefore a solution can easily be found via shooting. In three dimension the profile also depends on the azimuthal angle and a different approach becomes necessary. In an early work [28], to solve this kind of system, the profile ansatz was decomposed into an orthonormal angular basis i.e., in terms of Legendre polynomial. However, the interaction terms in the potential do mix such harmonics, leading to a complicated coupled system, which requires a by-hands truncation in order to be solved. Ref. [28] showed a good convergence already with the inclusion of the first few harmonics.

Later, an explicit full-numerical solution for Q-balls with vortices was found using the FIDISOL/CADSOL. This is a professional package, written in Fortran 90, developed by a team in Karlsruhe Institute of Technogy. Its purpose is to solve two and three dimensional elliptic and parabolic partial differential equations.

While this package can be used to solve much more complex systems, e.g., the profile of boson stars including the gravitational field [122], the algorithm, namely the Newton-Raphson method, was easily implementable in C++ by myself, and the desired solution was obtained.

In general such algorithm allows one to solve the following partial differential equation (written schematically):

$$P(r,\theta,\varphi,\varphi_r,\varphi_\theta,\varphi_{rr},\varphi_{\theta\theta},\varphi_{r\theta}) = 0, \tag{A.1}$$

where r,θ are the coordinates, φ the profile of the field and pedix denote its derivatives with respect to the coordinates.

This method is suitable for boundary problems on a $N_r \times N_\theta$ grid. However, the biggest (and only) disadvantage, is that it requires an initial ansatz for the solution. Such solution must indeed respect the boundary condition. Moreover, if it is too different from the exact solution, there will be no convergence. It should be noted that in most practical cases, however, it is very easy to come up with a physically well-motivated ansatz, which, by experience, leads to the right solution.

The algorithm can be summarized as follow:

- The initial ansatz $\varphi^{(0)}$ is not an exact solution to (A.1) i.e.
$$P(\varphi^{(0)}) \neq 0. \tag{A.2}$$
- Define a new solution
$$\varphi^{(1)} = \varphi^{(0)} + \delta\varphi^{(0)} \tag{A.3}$$
and assume this to be an exact solution to (A.1), i.e., $P(\varphi^{(1)}) = 0$.
- Expand $P(\varphi^{(1)} = 0$ for small $\delta\varphi^{(0)}$ to first order, i.e.,
$$0 = P(\varphi^{(1)}) = P(\varphi^{(0)} + \delta\varphi^{(0)}) \simeq P(\varphi^{(0)}) + \frac{\partial P}{\partial\varphi}(\varphi^{(0)})\delta\varphi^{0} \tag{A.4}$$
- Obtain $\varphi^{(1)}$ via (A.4). This consists of solving a linear system, for which different methods exist.
- Set the new solution to be the starting ansatz $\varphi^{(0)} = \varphi^{(1)}$ and go back to the first step.
- Keep iterating the above points until $P(\varphi^{(0)})$ is smaller than a prescribed initial value.

If the last point is fulfilled, the algorithm converged to the desired solution.

Notice that in order to derive (A.4), the derivative of P with respect to φ must be specified.

Appendix B

Fields equation for the confined monopoles

We write here explicitly the equations of motion we solve for the $SU(2)$ monopole/anti-monopole system, used for the numerical simulation

$$\partial_t^2\varphi^a = \nabla^2\varphi^a - g\epsilon^{abc}\partial_i\phi^b W_i^c - g\epsilon^{abc}(D_i\varphi)^b W_i^c - \lambda(\varphi^b\varphi^b - \eta^2)\varphi^a - g\epsilon^{abc}\varphi^b\Gamma^c - c\psi^\dagger\sigma^a\psi, \tag{B.1}$$

$$\partial_t^2\psi^\alpha = \nabla^2\psi^\alpha - \frac{g^2}{4}W_i^a W_i^a\psi^\alpha - i\frac{g}{2}\Gamma^a(\sigma^a\psi)^\alpha - igW_i^a(\sigma^a\partial_i\psi)^\alpha - c\varphi^a\sigma^a\psi^\alpha - \tilde{\lambda}(\psi^\dagger\psi - v^2)\psi^\alpha, \tag{B.2}$$

$$\begin{aligned}\partial_t W_{0i}^a &= \nabla^2 W_i^a + g\epsilon^{abc}W_j^b\partial_j W_i^c - g\epsilon^{abc}W_j^b W_{ij}^c - D_i\Gamma^a - g\epsilon^{abc}\varphi^b(D_i\varphi)^c + \\ &\quad - \frac{1}{2}g^2\psi^\dagger\psi W_i^a - ig\psi^\dagger\sigma^a\partial_i\psi,\end{aligned} \tag{B.3}$$

$$\partial_t\Gamma^a = \partial_i W_{0i}^a - g_p^2\left[\partial_i(W_{0i}^a) + g\epsilon^{abc}W_i^b W_{0i}^c + g\epsilon^{abc}\varphi^b(D_t\varphi)^c + ig\psi^\dagger\sigma^a\partial_t\psi\right], \tag{B.4}$$

where we are using the temporal gauge, $W_0^a = 0$, $\Gamma^a = \partial_i W_i^a$ are introduced as new variables, and $g_p^2 = 1.5$ is a numerical parameter that we can choose to ensure numerical stability. The equations were evolved with a Cranck-Nicolson leapfrog algorithm combined with absorbing boundary conditions [123].

Bibliography

[1] Jacob D. Bekenstein. Black holes and entropy. *Phys. Rev. D*, 7:2333–2346, 1973.

[2] S. W. Hawking. Particle Creation by Black Holes. *Commun. Math. Phys.*, 43:199–220, 1975. [Erratum: Commun.Math.Phys. 46, 206 (1976)].

[3] Don N. Page. Particle Emission Rates from a Black Hole: Massless Particles from an Uncharged, Nonrotating Hole. *Phys. Rev. D*, 13:198–206, 1976.

[4] Gia Dvali. Entropy Bound and Unitarity of Scattering Amplitudes. *JHEP*, 03:126, 2021.

[5] Gia Dvali, Oleg Kaikov, and Juan Sebastián Valbuena Bermúdez. How Special Are Black Holes? Correspondence with saturons in generic theories. 12 2021.

[6] Gia Dvali. Area Law Saturation of Entropy Bound from Perturbative Unitarity in Renormalizable Theories. *Fortsch. Phys.*, 69(1):2000090, 2021.

[7] Gia Dvali. Unitarity Entropy Bound: Solitons and Instantons. *Fortsch. Phys.*, 69(1):2000091, 2021.

[8] Gia Dvali, Florian Kühnel, and Michael Zantedeschi. Vortexes in Black Holes. 12 2021.

[9] Gia Dvali and Otari Sakhelashvili. Black-Hole-Like Saturons in Gross-Neveu. 11 2021.

[10] David J. Gross and Andre Neveu. Dynamical Symmetry Breaking in Asymptotically Free Field Theories. *Phys. Rev. D*, 10:3235, 1974.

[11] Gia Dvali and Raju Venugopalan. Classicalization and unitarization of wee partons in QCD and Gravity: The CGC-Black Hole correspondence. 6 2021.

[12] Francois Gelis, Edmond Iancu, Jamal Jalilian-Marian, and Raju Venugopalan. The Color Glass Condensate. *Ann. Rev. Nucl. Part. Sci.*, 60:463–489, 2010.

[13] Sidney R. Coleman. Q-balls. *Nucl. Phys. B*, 262(2):263, 1985. [Addendum: Nucl.Phys.B 269, 744 (1986)].

[14] Alexander Kusenko. Small Q balls. *Phys. Lett. B*, 404:285, 1997.

[15] Gerard 't Hooft. A Planar Diagram Theory for Strong Interactions. *Nucl. Phys. B*, 72:461, 1974.

[16] Lasha Berezhiani and Michael Zantedeschi. Evolution of coherent states as quantum counterpart of classical dynamics. *Phys. Rev. D*, 104(8):085007, 2021.

[17] Lasha Berezhiani, Giordano Cintia, and Michael Zantedeschi. Background-field method and initial-time singularity for coherent states. *Phys. Rev. D*, 105(4):045003, 2022.

[18] Gia Dvali and Cesar Gomez. Black Holes as Critical Point of Quantum Phase Transition. *Eur. Phys. J. C*, 74:2752, 2014.

[19] Gia Dvali and Cesar Gomez. Black Hole's Quantum N-Portrait. *Fortsch. Phys.*, 61:742–767, 2013.

[20] Gia Dvali and Cesar Gomez. Quantum Compositeness of Gravity: Black Holes, AdS and Inflation. *JCAP*, 01:023, 2014.

[21] A. Kovtun and M. Zantedeschi. Breaking BEC. *JHEP*, 07:212, 2020.

[22] A. Kovtun and M. Zantedeschi. Breaking BEC: Quantum evolution of unstable condensates. *Phys. Rev. D*, 105(8):085019, 2022.

[23] T. D. Lee and Y. Pang. Nontopological solitons. *Phys. Rept.*, 221:251–350, 1992.

[24] G. R. Dvali, Alexander Kusenko, and Mikhail E. Shaposhnikov. New physics in a nutshell, or Q ball as a power plant. *Phys. Lett. B*, 417:99–106, 1998.

[25] A. Vilenkin and E. P. S. Shellard. *Cosmic Strings and Other Topological Defects*. Cambridge University Press, 7 2000.

[26] Lucas G. Collodel, Burkhard Kleihaus, and Jutta Kunz. Structure of rotating charged boson stars. *Phys. Rev. D*, 99(10):104076, 2019.

[27] Chan-ju Kim, Seyong Kim, and Yoon-bai Kim. Global nontopological vortices. *Phys. Rev. D*, 47:5434–5443, 1993.

[28] Mikhail S. Volkov and Erik Wohnert. Spinning Q balls. *Phys. Rev. D*, 66:085003, 2002.

[29] G. R. Dvali and Goran Senjanovic. Topologically stable electroweak flux tubes. *Phys. Rev. Lett.*, 71:2376–2379, 1993.

[30] Ana Achucarro, Ruth Gregory, and Konrad Kuijken. Abelian Higgs hair for black holes. *Phys. Rev. D*, 52:5729–5742, 1995.

[31] T. Vachaspati and A. Achucarro. Semilocal cosmic strings. *Phys. Rev. D*, 44:3067–3071, 1991.

[32] Jonathan C. McKinney, Alexander Tchekhovskoy, and Roger D. Blandford. General Relativistic Magnetohydrodynamic Simulations of Magnetically Choked Accretion Flows around Black Holes. *Mon. Not. Roy. Astron. Soc.*, 423:3083, 2012.

[33] R. D. Blandford and R. L. Znajek. Electromagnetic extractions of energy from Kerr black holes. *Mon. Not. Roy. Astron. Soc.*, 179:433–456, 1977.

[34] Kazunori Akiyama et al. First M87 Event Horizon Telescope Results. VIII. Magnetic Field Structure near The Event Horizon. *Astrophys. J. Lett.*, 910(1):L13, 2021.

[35] Eric Adelberger, Gia Dvali, and Andrei Gruzinov. Photon mass bound destroyed by vortices. *Phys. Rev. Lett.*, 98:010402, 2007.

[36] Wayne Hu, Rennan Barkana, and Andrei Gruzinov. Cold and fuzzy dark matter. *Phys. Rev. Lett.*, 85:1158–1161, 2000.

[37] Lam Hui, Jeremiah P. Ostriker, Scott Tremaine, and Edward Witten. Ultralight scalars as cosmological dark matter. *Phys. Rev. D*, 95(4):043541, 2017.

[38] Raffaella Margutti et al. The Electromagnetic Counterpart of the Binary Neutron Star Merger LIGO/VIRGO GW170817. V. Rising X-ray Emission from an Off-Axis Jet. *Astrophys. J. Lett.*, 848(2):L20, 2017.

[39] Gia Dvali, Florian Kühnel, and Michael Zantedeschi. Primordial black holes from confinement. *Phys. Rev. D*, 104(12):123507, 2021.

[40] B. P. Abbott et al. Binary Black Hole Mergers in the first Advanced LIGO Observing Run. *Phys. Rev. X*, 6(4):041015, 2016. [Erratum: Phys.Rev.X 8, 039903 (2018)].

[41] R. Abbott et al. Tests of general relativity with binary black holes from the second LIGO-Virgo gravitational-wave transient catalog. *Phys. Rev. D*, 103(12):122002, 2021.

[42] Bernard Carr and Florian Kühnel. Primordial Black Holes as Dark Matter: Recent Developments. *Ann. Rev. Nucl. Part. Sci.*, 70:355–394, 2020.

[43] Tomohiro Matsuda. Primordial black holes from monopoles connected by strings. *Astropart. Phys.*, 30:333–337, 2009.

[44] Zaven Arzoumanian et al. The NANOGrav 12.5 yr Data Set: Search for an Isotropic Stochastic Gravitational-wave Background. *Astrophys. J. Lett.*, 905(2):L34, 2020.

[45] Bernard Carr, Sebastien Clesse, Juan García-Bellido, and Florian Kühnel. Cosmic conundra explained by thermal history and primordial black holes. *Phys. Dark Univ.*, 31:100755, 2021.

[46] Stephen Hawking. Gravitationally collapsed objects of very low mass. *Mon. Not. Roy. Astron. Soc.*, 152:75, 1971.

[47] Yakov Zel'dovich and I. D. Novikov. The Hypothesis of Cores Retarded during Expansion and the Hot Cosmological Model. *Sov. astron.*, 10:602–603, 1967.

[48] Bernard J. Carr. The Primordial black hole mass spectrum. *Astrophys. J.*, 201:1–19, 1975.

[49] Matthew Choptuik. Universality and scaling in gravitational collapse of a massless scalar field. *Phys. Rev. Lett.*, 70:9–12, 1993.

[50] Tatsuhiko Koike, Takashi Hara, and Satoshi Adachi. Critical behavior in gravitational collapse of radiation fluid: A Renormalization group (linear perturbation) analysis. *Phys. Rev. Lett.*, 74:5170–5173, 1995.

[51] Jens Niemeyer and Karsten Jedamzik. Near-Critical Gravitational Collapse and the Initial Mass Function of Primordial Black Holes. *Phys. Rev. Lett.*, 80:5481–5484, 1998.

[52] Charles Evans and Jason Coleman. Observation of critical phenomena and selfsimilarity in the gravitational collapse of radiation fluid. *Phys. Rev. Lett.*, 72:1782–1785, 1994.

[53] Carsten Gundlach. Critical phenomena in gravitational collapse. *Living Rev. Rel.*, 2:4, 1999.

[54] Ilia Musco and John C. Miller. Primordial black hole formation in the early universe: critical behaviour and self-similarity. *Class. Quant. Grav.*, 30:145009, 2013.

[55] Florian Kühnel, Cornelius Rampf, and Marit Sandstad. Effects of Critical Collapse on Primordial Black-Hole Mass Spectra. *Eur. Phys. J.*, C76(2):93, 2016.

[56] V. De Luca, G. Franciolini, P. Pani, and A. Riotto. The evolution of primordial black holes and their final observable spins. *JCAP*, 04:052, 2020.

[57] Takeshi Chiba and Shuichiro Yokoyama. Spin Distribution of Primordial Black Holes. *PTEP*, 2017(8):083E01, 2017.

[58] Mehrdad Mirbabayi, Andrei Gruzinov, and Jorge Noreña. Spin of Primordial Black Holes. *JCAP*, 03:017, 2020.

[59] V. De Luca, V. Desjacques, G. Franciolini, A. Malhotra, and A. Riotto. The initial spin probability distribution of primordial black holes. *JCAP*, 05:018, 2019.

[60] Tomohiro Harada, Chul-Moon Yoo, Kazunori Kohri, and Ken-Ichi Nakao. Spins of primordial black holes formed in the matter-dominated phase of the Universe. *Phys. Rev. D*, 96(8):083517, 2017. [Erratum: Phys.Rev.D 99, 069904 (2019)].

[61] Heling Deng and Alexander Vilenkin. Primordial black hole formation by vacuum bubbles. *JCAP*, 12:044, 2017.

[62] Heling Deng. Primordial black hole formation by vacuum bubbles. Part II. *JCAP*, 09:023, 2020.

[63] G. W. Gibbons and S. W. Hawking. Cosmological Event Horizons, Thermodynamics, and Particle Creation. *Phys. Rev. D*, 15:2738–2751, 1977.

[64] Rama Basu, Alan H. Guth, and Alexander Vilenkin. Quantum creation of topological defects during inflation. *Phys. Rev. D*, 44:340–351, 1991.

[65] Bernard Carr, Martti Raidal, Tommi Tenkanen, Ville Vaskonen, and Hardi Veermäe. Primordial black hole constraints for extended mass functions. *Phys. Rev. D*, 96(2):023514, 2017.

[66] Ilia Musco, John C. Miller, and Alexander G. Polnarev. Primordial black hole formation in the radiative era: Investigation of the critical nature of the collapse. *Class. Quant. Grav.*, 26:235001, 2009.

[67] Albert Escrivà, Cristiano Germani, and Ravi K. Sheth. Universal threshold for primordial black hole formation. *Phys. Rev. D*, 101(4):044022, 2020.

[68] Ilia Musco, Valerio De Luca, Gabriele Franciolini, and Antonio Riotto. Threshold for primordial black holes. II. A simple analytic prescription. *Phys. Rev. D*, 103(6):063538, 2021.

[69] Florian Kühnel and Marit Sandstad. Ellipsoidal collapse and primordial black hole formation. *Phys. Rev. D*, 94(6):063514, 2016.

[70] Kaushala Bandara, David Crampton, and Luc Simard. A Relationship Between Supermassive Black Hole Mass and the Total Gravitational Mass of the Host Galaxy. *Astrophys. J*, 704(2):1135–1145, October 2009.

[71] Marta Volonteri. Formation of Supermassive Black Holes. *Astron. Astrophys. Rev.*, 18:279–315, 2010.

[72] Pasquale D. Serpico, Vivian Poulin, Derek Inman, and Kazunori Kohri. Cosmic microwave background bounds on primordial black holes including dark matter halo accretion. *Phys. Rev. Res.*, 2(2):023204, 2020.

[73] Christopher J. Conselice, Aaron Wilkinson, Kenneth Duncan, and Alice Mortlock. The evolution of galaxy number density at $z < 8$ and its implications. *Astrophys. J.*, 830(2):83, 2016.

[74] José Luis Bernal, Alvise Raccanelli, Licia Verde, and Joseph Silk. Signatures of primordial black holes as seeds of supermassive black holes. *JCAP*, 05:017, 2018. [Erratum: JCAP 01, E01 (2020)].

[75] Fabio Pacucci, Priyamvada Natarajan, Marta Volonteri, Nico Cappelluti, and C. Megan Urry. Conditions for Optimal Growth of Black Hole Seeds. *Astrophys. J. Lett.*, 850(2):L42, 2017.

[76] Bernard Carr, Florian Kühnel, and Luca Visinelli. Constraints on Stupendously Large Black Holes. *Mon. Not. Roy. Astron. Soc.*, 501(2):2029–2043, 2021.

[77] Stephen W Hawking. Black hole explosions? *Nature*, 248(5443):30–31, 1974.

[78] Stephen W Hawking. Particle creation by black holes. *Communications in mathematical physics*, 43(3):199–220, 1975.

[79] Gia Dvali. A Microscopic Model of Holography: Survival by the Burden of Memory. 10 2018.

[80] Gia Dvali, Lukas Eisemann, Marco Michel, and Sebastian Zell. Black hole metamorphosis and stabilization by memory burden. *Phys. Rev. D*, 102(10):103523, 2020.

[81] Xavier Martin and Alexander Vilenkin. Gravitational radiation from monopoles connected by strings. *Phys. Rev. D*, 55:6054–6060, 1997.

[82] Xavier Martin and Alexander Vilenkin. Gravitational wave background from hybrid topological defects. *Phys. Rev. Lett.*, 77:2879–2882, 1996.

[83] Eugeny Babichev, V. Dokuchaev, and M. Kachelriess. Gravitational radiation from rotating monopole-string systems. *Phys. Rev. D*, 71:044028, 2005.

[84] Louis Leblond, Benjamin Shlaer, and Xavier Siemens. Gravitational Waves from Broken Cosmic Strings: The Bursts and the Beads. *Phys. Rev. D*, 79:123519, 2009.

[85] Wilfried Buchmuller, Valerie Domcke, and Kai Schmitz. Stochastic gravitational-wave background from metastable cosmic strings. 7 2021.

[86] Thibault Damour and Alexander Vilenkin. Gravitational wave bursts from cusps and kinks on cosmic strings. *Phys. Rev. D*, 64:064008, 2001.

[87] Pierre Touboul et al. MICROSCOPE Mission: First Results of a Space Test of the Equivalence Principle. *Phys. Rev. Lett.*, 119(23):231101, 2017.

[88] Joel Bergé, Philippe Brax, Gilles Métris, Martin Pernot-Borràs, Pierre Touboul, and Jean-Philippe Uzan. MICROSCOPE Mission: First Constraints on the Violation of the Weak Equivalence Principle by a Light Scalar Dilaton. *Phys. Rev. Lett.*, 120(14):141101, 2018.

[89] Massimo Blasone, Salvatore Capozziello, Gaetano Lambiase, and Luciano Petruzziello. Equivalence principle violation at finite temperature in scalar-tensor gravity. *Eur. Phys. J. Plus*, 134(4):169, 2019.

[90] R. W. Hellings and G. S. Downs. Upper limits on the isotropic gravitational radiation background from pulsar timing analysis. *Astrophys. J. Lett.*, 265:L39–L42, February 1983.

[91] G. R. Dvali. Removing the cosmological bound on the axion scale. 5 1995.

[92] Veniamin Berezinsky, Xavier Martin, and Alexander Vilenkin. High-energy particles from monopoles connected by strings. *Phys. Rev. D*, 56:2024–2034, 1997.

[93] J. Polchinski. *String theory. Vol. 2: Superstring theory and beyond.* Cambridge Monographs on Mathematical Physics. Cambridge University Press, 12 2007.

[94] G. R. Dvali and S. H. Henry Tye. Brane inflation. *Phys. Lett. B*, 450:72–82, 1999.

[95] G. R. Dvali, Q. Shafi, and S. Solganik. D-brane inflation. In *4th European Meeting From the Planck Scale to the Electroweak Scale*, 5 2001.

[96] G. R. Dvali. Infrared hierarchy, thermal brane inflation and superstrings as superheavy dark matter. *Phys. Lett. B*, 459:489–496, 1999.

[97] Saswat Sarangi and S. H. Henry Tye. Cosmic string production towards the end of brane inflation. *Phys. Lett. B*, 536:185–192, 2002.

[98] Edmund J. Copeland, Robert C. Myers, and Joseph Polchinski. Cosmic F and D strings. *JHEP*, 06:013, 2004.

[99] Gia Dvali and Alexander Vilenkin. Formation and evolution of cosmic D strings. *JCAP*, 03:010, 2004.

[100] Guillem Domènech and Shi Pi. NANOGrav Hints on Planet-Mass Primordial Black Holes. 10 2020.

[101] Clifford M. Will and Nicolas Yunes. Testing alternative theories of gravity using LISA. *Class. Quant. Grav.*, 21:4367, 2004.

[102] Ignatios Antoniadis, S. Dimopoulos, and G. R. Dvali. Millimeter range forces in superstring theories with weak scale compactification. *Nucl. Phys. B*, 516:70–82, 1998.

[103] G. R. Dvali and Matias Zaldarriaga. Changing alpha with time: Implications for fifth force type experiments and quintessence. *Phys. Rev. Lett.*, 88:091303, 2002.

[104] G. Dvali, V. S. Valbuena, and M. Zantedeschi.

[105] A. A. Abrikosov. On the Magnetic properties of superconductors of the second group. *Sov. Phys. JETP*, 5:1174–1182, 1957.

[106] Holger Bech Nielsen and P. Olesen. Vortex Line Models for Dual Strings. *Nucl. Phys. B*, 61:45–61, 1973.

[107] Yoichiro Nambu. Strings, Monopoles and Gauge Fields. *Phys. Rev. D*, 10:4262, 1974.

[108] S. Mandelstam. Vortices and Quark Confinement in Nonabelian Gauge Theories. *Phys. Rept.*, 23:245–249, 1976.

[109] Gerard 't Hooft. On the Phase Transition Towards Permanent Quark Confinement. *Nucl. Phys. B*, 138:1–25, 1978.

[110] J. Antoniadis et al. The International Pulsar Timing Array second data release: Search for an isotropic Gravitational Wave Background. *Mon. Not. Roy. Astron. Soc.*, 510(4), 2022.

[111] Louis Leblond, Benjamin Shlaer, and Xavier Siemens. Gravitational Waves from Broken Cosmic Strings: The Bursts and the Beads. *Phys. Rev. D*, 79:123519, 2009.

[112] G. 't Hooft. Magnetic Monopoles in Unified Theories. In *17th International Conference on High-Energy Physics*, pages III.84–85, 1974.

[113] Alexander M. Polyakov. Compact Gauge Fields and the Infrared Catastrophe. *Phys. Lett. B*, 59:82–84, 1975.

[114] Ayush Saurabh and Tanmay Vachaspati. Monopole-antimonopole Interaction Potential. *Phys. Rev. D*, 96(10):103536, 2017.

[115] Clifford Henry Taubes. The Existence of a Nonminimal Solution to the SU(2) Yang-Mills Higgs Equations on R**3. *Commun. Math. Phys.*, 86:257, 1982.

[116] N. S. Manton. Topology in the Weinberg-Salam Theory. *Phys. Rev. D*, 28:2019, 1983.

[117] Yoichiro Nambu. String-Like Configurations in the Weinberg-Salam Theory. *Nucl. Phys. B*, 130:505, 1977.

[118] Tanmay Vachaspati. Monopole-Antimonopole Scattering. *Phys. Rev. D*, 93(4):045008, 2016.

[119] Steven Weinberg. *Gravitation and Cosmology: Principles and Applications of the General Theory of Relativity.* John Wiley and Sons, New York, 1972.

[120] Burkhard Kleihaus and Jutta Kunz. A Monopole - anti-monopole solution of the SU(2) Yang-Mills-Higgs model. *Phys. Rev. D*, 61:025003, 2000.

[121] Tanmay Vachaspati and George B. Field. Electroweak string configurations with baryon number. *Phys. Rev. Lett.*, 73:373–376, 1994.

[122] Jorge F. M. Delgado, Carlos A. R. Herdeiro, Eugen Radu, and Helgi Runarsson. Kerr–Newman black holes with scalar hair. *Phys. Lett. B*, 761:234–241, 2016.

[123] Moshe Israeli and Steven A. Orszag. Approximation of radiation boundary conditions. *Journal of Computational Physics*, 41(1):115–135, 1981.

Acknowledgements

First and foremost my gratitude goes towards my supervisor Gia Dvali. His insights and constant pursuit of a clear and simple understanding of physical phenomena was of great inspiration. Interacting with him, and with the group he formed, not only was lots of fun, but it also deeply shaped the way I approach research, providing an unvaluable set of skills which I will always carry with myself. Gia also proved to be a formidable allied whenever I ran into a troubled spot, providing always a fulmineous, but extremely balanced and thought through advice. Thanks.

Deep thanks also go to Goran Senjanović, which joined our group during the second half of my doctoral studies. He introduced me and taught me about Grand Unified Theories, sharing with me his personal, unique and very passionate views on physics (and the World). What started as a mere exploration guided by curiosity, rapidly turned into a fruitful collaboration whose output makes me proud.

Further thanks goes to all the group members I crossed path with, among which I found several collaborators (in no particular order): Lasha Berezhiani, Florian Kühnel, Juan Valbuena, Andrei Kovtun and Giordano Cintia. My constantly ongoing discussion with them helped me growing as a physicist and played a substantial role throughout my PhD.

Last but not least, I wish to express my very profound gratitude to Katia Hochstetter and Haruki for providing me with unfailing support and continuous encouragement throughout all these years. This would not have been possible without them.

Thank you
Michael